

# Fully probabilistic design for knowledge fusion between Bayesian filters under uniform disturbances

Lenka Kuklišová Pavelková<sup>a,\*</sup>, Ladislav Jirsa<sup>a</sup>, Anthony Quinn<sup>a,b</sup>

<sup>a</sup>*Czech Academy of Sciences, Institute of Information Theory and Automation  
Pod vodárenskou věží 4, Prague, Czech Republic*

<sup>b</sup>*Trinity College Dublin, the University of Dublin, Ireland*

---

## Abstract

This paper considers the problem of Bayesian transfer learning-based knowledge fusion between linear state-space processes driven by uniform state and observation noise processes. The target task conditions on probabilistic state predictor(s) supplied by the source filtering task(s) to improve its own state estimate. A joint model of the target and source(s) is not required and is not elicited. The resulting decision-making problem for choosing the optimal conditional target filtering distribution under incomplete modelling is solved via fully probabilistic design (FPD), i.e. via appropriate minimization of Kullback-Leibler divergence (KLD). The resulting FPD-optimal target learner is robust, in the sense that it can reject poor-quality source knowledge. In addition, the fact that this Bayesian transfer learning (BTL) scheme does not depend on a model of interaction between the source and target tasks ensures robustness to the misspecification of such a model. The latter is a problem that affects conventional transfer learning methods. The properties of the proposed BTL scheme are demonstrated via extensive simulations, and in comparison with two contemporary alternatives.

### *Keywords:*

knowledge fusion, Bayesian transfer learning, fully probabilistic design, state-space models, bounded noise, Bayesian inference

---

## 1. Introduction

Methods of data and information fusion are receiving much attention at present, because of their range of applications in industry 4.0, in the navigation and localization problems, in sensor networks, robotics, and so on [1] – [3].

The terms *data* fusion and *information* fusion are often used as synonyms. However, in some scenarios, the term data fusion is used for raw data that are obtained directly from the sensors, while the term information fusion concerns

---

\*Corresponding author. E-mail address: pavelkov@utia.cas.cz.

processed or transformed data. Other terms associated with data fusion include data combination, data aggregation, multi-sensor data fusion, and sensor fusion [4].

Data fusion techniques combine multiple sources in order to obtain improved (less expensive, higher quality, or more relevant) inferences and decisions compared to a single source. These techniques can be classified into three non-exclusive categories: (i) data association, (ii) state estimation, and (iii) decision fusion [4]. In this paper, we focus on state estimation methods.

Conventional data fusion methods work with multiple data channels from one common domain, and originating from the same source. In contrast, cross-domain fusion methods work with data in different domains, but related by a common latent object [5]. Data from different domains cannot be merged directly. Instead, knowledge—or “information” above—has to be extracted from these data and only then fused. One method of knowledge fusion is transfer learning, also known as knowledge transfer. This framework aims to extract knowledge from a source domain via a source learning task and to use it in the target domain with a given target learning task. The domains or tasks may differ between the source and target [6]. Examples of successful deployment of transfer learning in data fusion are found in [7] – [10]. In accordance with the DIKW classification scheme proposed in [11], we will refer to transfer learning-based fusion as knowledge fusion.

The performance of transfer learning methods can be improved using computational intelligence [12]. Bayesian inference provides a consistent approach to building in computational intelligence. It does so via probabilistic uncertainty quantification in decision-making, taking into consideration the uncertainty associated with model parameters, as well as, the uncertainty associated with combining multiple sources of data. In the Bayesian transfer learning (BTL) framework—to be championed in this paper—the source and target can be related through a joint prior distribution, as in [13] – [15]. BTL usually adopts a complete stochastic modelling framework, such as Bayesian networks [16], Bayesian neural networks [14] or hierarchical Bayesian approaches [17]. As already noted, these methods require a complete model of source-target interaction. In contrast, in [18], BTL is defined as the task of conditioning a target probability distribution on a transferred source distribution. A dual-modeller framework is adopted, where the target modeller conditions on a probabilistic data predictor provided by an independent local source modeller. No joint interaction model between the source and target is specified, and so the source-conditional target distribution is non-unique and can be optimized in this incomplete modelling scenario. The target undertakes this distributional decision-making task optimally, by minimizing an approximate Kullback-Leibler divergence [19]. This generalized approach to Bayesian conditioning in incomplete modelling scenario is known as fully probabilistic design [20].

Our aim in this paper is to derive a BTL algorithm for knowledge fusion that will use knowledge from several source state-space filters to improve state estimation in a single target state-space filter. All (observational and modelling) uncertainties are assumed to be bounded. State estimation under bounded

noises represents a significant focus for state filtering methods, since, in practice, the statistical properties of noises are rarely known, with only their bounds being available. They avoid the adoption of unbounded noises, that can lead to over-conservative design [21]. To the best of our knowledge, the topic of BTL-based multi-task/filter state estimation with bounded noises has not yet been addressed in the literature, except in the author’s previous publications [22, 23]. In those papers, BTL between a *pair* of filters affected by bounded noises is presented. The source knowledge is represented by a bounded output (i.e. data) predictor. The optimal target state filtering distribution is then designed via FPD. In [22], the support of the state inference is an orthotope, while in [23], it is relaxed to a parallelotope.

There are fusion techniques for state estimation with bounded noises, but these are conventional fusion methods as defined above. Data fusion methods using set membership estimation are addressed, for instance, in [24] – [28]. In [29], set membership and stochastic estimation are combined. In [30], local Kalman-like estimates are computed in the presence of bounded noises. Particle filters [31] can also effectively solve the Bayesian estimation problem with bounded noises. However, they are computationally demanding. When used in data fusion context, reduced computational complexity is obtained in [32]. In [33] and [34], particle filtering techniques and set membership approaches are combined.

The current paper significantly extends and formalizes results on BTL reported in the above-mentioned authors’ papers [22] and [23]. Both of those papers report an improvement in target performance in the case of concentrated source knowledge (positive transfer) and rejection of diffuse source knowledge (robust transfer). However, the improvement was only minor compared to the performance of the isolated target, whereas *ad hoc* proposed variants exhibited significantly improved positive transfer. In the current paper, we formalize the above-mentioned informal variant, showing it to be FPD-optimal. The task of transfer learning-based knowledge fusion with bounded noises is solved in the case where the transferred knowledge is the source’s probabilistic state predictor. An extension to multiple sources is also provided in this paper.

The paper is organized as follows: This section ends with a brief summary of the notation used throughout the paper. Section 2 presents the general problem of FPD-optimal Bayesian state inference and estimation in the target, conditioning on transferred knowledge from a source in the form of the probabilistic state predictor. In Section 3, these general results are specialized to source and target state-space models with uniform noises, and are finally extended to the case of multiple sources in Section 3.3. Section 4 provides the extensive simulation evidence to illustrate the performance of our FPD-optimal BTL scheme. Comparison with a contemporary (non-Bayesian) fusion method for uniformly driven state-space models is also provided, as well as comparison with a completely modelled Bayesian network approach. Section 5 concludes the paper. The proofs of all the theorems are provided in Appendix A.

**Notation:** Matrices are denoted by capital letters (e.g.  $A$ ), vectors and scalars by lowercase letters (e.g.  $b$ ).  $A_{ij}$  is the (i,j)-th element of matrix  $A$ .  $A_i$  denotes the  $i$ -th row of  $A$ .  $\ell_x$  denotes the length of a (column) vector  $x$ , and  $\mathbb{X}$  denotes the set of  $x$ . Vector inequalities, e.g.  $\underline{x} < \bar{x}$ , as well as vector maximum and minimum operators, e.g.  $\min\{x, y\}$ , are meant entry-wise.  $I$  is the identity matrix.  $\chi_x(\mathbb{X})$  is the set indicator, equalling 1 if  $x \in \mathbb{X}$  and 0 otherwise.  $x_t$  is the value of a time-variant column vector  $x$ , at a discrete time instant,  $t \in \mathbb{T} \equiv \{1, 2, \dots, \bar{t}\}$ ;  $x_{t;i}$  is the  $i$ -th entry of  $x_t$ ;  $x(t) \equiv \{x_t, x_{t-1}, \dots, x_1\}$ .  $\|x\|_2$  is the Euclidean norm of  $x$  and  $\|x\|_\infty$  is the  $H_\infty$  norm of  $x$ . Note that no notational distinction is made between a random variable and its realisation,  $X(\omega) \equiv x$ . The context will make clear which is meant.

## 2. FPD-optimal Bayesian transfer learning (FPD-BTL)

Assume two stochastically independent modellers, the source (with subscript S) and the target (without subscript), each modelling their local environment. Here, we will formulate the task of FPD-optimal Bayesian transfer learning (FPD-BTL) between this source and target, the aim being to improve the target’s model of its local environment via transfer of probabilistic knowledge from the source’s local environment, as depicted in Figure 1.

Before addressing the two-task context, let us recall the state estimation problem (filtering) for an *isolated* target, i.e. in the absence of knowledge transfer from a source.

In the Bayesian filtering framework [35], a system of interest is described by the following probability density functions (pdfs):

$$\begin{aligned} &\text{prior pdf } f(x_1), \text{ observation model } f(y_t|x_t), t \in \mathbb{T} \\ &\text{and time evolution model } f(x_{t+1}|x_t, u_t), t \in \mathbb{T} \setminus \bar{t}. \end{aligned} \quad (1)$$

Here,  $y_t$  is an  $\ell_y$ -dimensional observable output,  $u_t$  is an optional  $\ell_u$ -dimensional known (exogenous) system input, and  $x_t$  is an  $\ell_x$ -dimensional unobservable (hidden) system state. We assume that (i) the hidden state process,  $x_t$ , satisfies the Markov property; (ii) no direct relationship between input and output exists in the observation model; and (iii) the optional inputs constitute of a known sequence  $u_t, t \in \mathbb{T}$ , as already stated.

Bayesian filtering, i.e. the inference task of learning the unknown state process,  $x_t$ , given the data history  $d(t)$ , involves sequential computation of the posterior pdf,  $f(x_t|d(t))$ . Specifically,  $d(t)$  is a (multivariate) sequence of observed data,  $d_t = \{y_t, u_t\}$ ,  $t \in \mathbb{T}$ . Evolution of  $f(x_t|d(t))$  is described by a two-step recursion (the data update and time update) initialized with the prior pdf,  $f(x_1) \equiv f(x_1|d(0))$  (1), and ending with a data update at the final time,  $t = \bar{t}$ .

The data update (Bayes’ rule) processes the latest datum,  $d_t$ :

$$f(x_t|d(t)) = \frac{f(y_t|x_t)f(x_t|d(t-1))}{\int_{\mathbb{X}_t} f(y_t|x_t)f(x_t|d(t-1)) dx_t}. \quad (2)$$

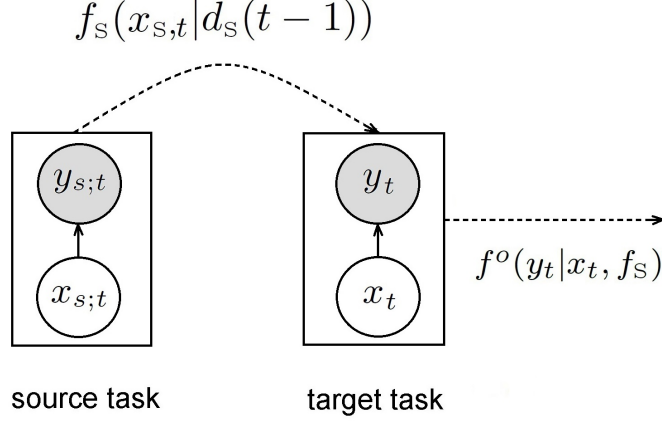


Figure 1: Bayesian transfer learning (BTL), involving probabilistic knowledge transfer from the source to the target Bayesian filter. The source filter transfers its state predictor,  $f_s(x_{s,t}|d_s(t-1))$ , statically at each time,  $t = 1, 2, \dots, \bar{t}$ , to the target filter to improve the target’s filtering performance. The source data,  $d_s(t)$ , are unobserved by the target, which computes an optimal conditional model of its local observations, i.e.  $f^o(y_t|x_t, f_s)$ , at each time,  $t$ . Probabilistic knowledge flow is depicted by dashed lines above.

The time update (marginalization) infers the evolution of the state at the next time:

$$f(x_{t+1}|d(t)) = \int_{\mathbb{X}_t} f(x_{t+1}|u_t, x_t) f(x_t|d(t)) dx_t. \quad (3)$$

Next, we return to two stochastically independent modellers, i.e. the source and target (Figure 1). Each filter models its local system,  $\{x_s, d_s\}$  and  $\{x, d\}$ , respectively. The target has access only to the (probabilistic) state predictor of the source,  $f_s(x_{s,t}|d_s(t-1))$ , but not to the actual data or states of the source (Figure 1).

In the isolated target task, the modeller’s complete knowledge about the evolution of its local state and output is expressed uniquely by the joint pdf (i.e. the numerator in (2)):

$$f(y_t, x_t|d(t-1)) = f(y_t|x_t) f(x_t|d(t-1)), \quad (4)$$

where  $x_t \in \mathbb{X}_t$  and  $y_t \in \mathbb{Y}_t|x_t$ .

Now, performing knowledge transfer as depicted in Figure 1, the target joint pdf (4) must be conditioned by the transferred source state predictor,  $f_s \equiv f_s(x_{s,t}|d_s(t-1))$ , and so the target’s knowledge-conditional joint pdf takes the form  $\check{f}(y_t, x_t|d(t-1), f_s)$ . Since no joint model of the source and target relationship is assumed, this pdf is non-unique, and unknown. Specifically, it is a variational quantity,  $f$ , in a function set,  $\mathbb{F}$ , of possible candidates, as follows:

$$\check{f} \equiv \check{f}(y_t, x_t|d(t-1), f_s) = \check{f}(y_t|x_t, d(t-1), f_s) \check{f}(x_t|d(t-1), f_s) \in \check{\mathbb{F}} \quad (5)$$

We now separately examine the two factors on the right-hand side of (5):

1. The factor  $\check{f}(x_t|d(t-1), f_s)$  represents the target's knowledge about its (local) state  $x_t$ , after transfer of the source's state predictor,  $f_s$ , to the target. The target chooses to accept the source's predictor as its own state model with *full* acceptance. The consequences of this definition will be discussed in Section 4.7. Based on this full acceptance, the target accepts that  $x_{s,t}$  and  $x_t$  are equal in distribution:

$$\check{f}(x_t|d(t-1), f_s) \equiv f_s(x_{s,t}|d_s(t-1)) \Big|_{x_{s,t} \rightarrow x_t} = f_s(x_t|d_s(t-1)). \quad (6)$$

In consequence, the factor (6) is fixed in (5).

2. The factor  $\check{f}(y_t|x_t, d(t-1), f_s)$  now remains as the only variational factor, being a consequence of the target's choice not to elicit an interaction model between the source and target (Figure 1). According to (1),  $f(y_t|x_t, d(t-1)) = f(y_t|x_t)$ , i.e. the observation model is conditionally independent, given  $x_t$ , of  $d(t-1)$ . This conditional independence is preserved by the knowledge transfer. Therefore,

$$\check{f}(y_t|x_t, d(t-1), f_s) \equiv \check{f}(y_t|x_t, f_s). \quad (7)$$

The main design—i.e. decision—problem for the target is now to choose an optimal form of (7).

Inserting (6) and (7) into (5):

$$\check{f} \equiv \check{f}(y_t, x_t|d(t-1), f_s) = \check{f}(y_t|x_t, f_s) f_s(x_t|d_s(t-1)), \quad (8)$$

where  $x_t \in \mathbb{X}_{s,t}$  and  $y_t \in \mathbb{Y}_t|x_t, f_s$ . The set,  $\check{\mathbb{F}}$ , of the target's admissible joint models,  $\check{f}$ , following knowledge transfer from the source, is therefore

$$\check{f} \in \check{\mathbb{F}} \equiv \{\text{set of models (8) with } f_s(x_t|\cdot) \text{ fixed and } \check{f}(y_t|\cdot) \text{ variational}\}. \quad (9)$$

The optimal pdf,  $f^o(y_t|x_t, f_s) \in \check{\mathbb{F}}$ , respecting both the transferred knowledge and the target filter behaviour, is sought using fully probabilistic design (FPD), which is an axiomatically justified procedure for distributional decision-making [36], [37]. It seeks  $\check{f} = f^o \in \check{\mathbb{F}}$ , being the joint pdf (8) that minimizes the Kullback-Leibler divergence (KLD) (below) [19] from  $\check{f}$  to the target's fixed ideal,  $f^I$ . This ideal is defined as (4), i.e. the joint pdf of the isolated target filter, modelling its behaviour prior to (i.e. without) the transfer of source knowledge. To summarize, the ideal pdf, and the knowledge-conditional pdf to be designed by the target are, according to (4), (8) and (9):

$$\text{ideal: } f^I \equiv f(y_t|x_t) f(x_t|d(t-1)), \quad (10)$$

$$\text{variational: } \check{f} \equiv \underbrace{\check{f}(y_t|x_t, f_s)}_{\text{to be optimized}} f_s(x_t|d_s(t-1)). \quad (11)$$

Recall that the KLD [19] from  $\check{f}$  to  $f^I$  is defined as

$$D(\check{f} \parallel f^I) = \mathbb{E}_{\check{f}} \left[ \ln \frac{\check{f}}{f^I} \right], \quad (12)$$

where  $\mathbb{E}_{\check{f}}$  denotes expectation with respect to  $\check{f}$ . FPD consists in minimizing this KLD (12) objective as a function of  $\check{f}(y_t|x_t, f_s)$  in (11), for the fixed ideal (10), i.e.

$$f^o(y_t|x_t, f_s) \equiv \arg \min_{\check{f}(y_t|x_t, f_s)} D(\check{f} \parallel f^I), \quad (13)$$

(13) conditions the target’s knowledge about future  $y_t$  on the transferred  $f_s$  in an FPD-optimal manner. For simplicity, the superscript  $o$  will be omitted in the resulting FPD-optimal pdf, i.e.  $f(y_t|x_t, f_s) \equiv f^o(y_t|x_t, f_s)$ .

We note the following:

- The transferred source knowledge,  $f_s(x_{s,t}|d_s(t-1))$ , can be elicited in various ways that are unknown to the target; e.g. as an empirical distribution of a quantity similar to  $x_t$ , or some unspecified distributional approximation, etc. [38]. In this paper, involving multiple state filtering tasks, we will assume that  $f_s(x_{s,t}|d_s(t-1))$  is the output of the source’s synchronized time update at  $t-1$  (3).
- In the authors’ previous publications [22], [23], [39], it was the source *data* predictor which was transferred. Instead, here, *for the first time*, it is the source state predictor,  $f_s(x_{s,t}|d_s(t-1))$ ,  $t \in \mathbb{T}$ , that is transferred. As we will see later, *this setting ensures robust knowledge transfer*.

Recall that our aim is to specialize FPD-optimal Bayesian transfer learning (FPD-BTL framework) defined in (10), (11), (13) to a pair of Bayesian filters under *bounded* observational and state noises. We now address this aim.

### 3. FPD-BTL between LSU-UOS filtering tasks

As noted in Section 1, we are specifically interested in knowledge processing among interacting Bayesian state-space filters with uniform noises (LSU models, see below). We therefore instantiate the FPD-optimal scheme (13) for conditioning the target’s observation model on the source’s transferred state predictor in this specific context. Firstly, in Section 3.1, we review the isolated LSU-UOS filter, and derive the approximate solution to the related state estimation problem. Then, the required instantiation of FPD-BTL to a pair of these LSU-UOS filters is presented in Section 3.2. In Section 3.3, the framework is extended to multiple LSU-UOS source filters, transferring probabilistic state knowledge to a single target.

### 3.1. LSU-UOS filtering task for the isolated target

The general stochastic system description in (1) is now instantiated as a linear state-space model [40]

$$y_t = Cx_t + v_t \quad \equiv \tilde{y}_t + v_t, \quad (14)$$

$$x_{t+1} = Ax_t + Bu_t + w_{t+1} \equiv \tilde{x}_{t+1} + w_{t+1}, \quad (15)$$

where  $x_t \in \mathbb{R}^{\ell_x}$ ,  $y_t \in \mathbb{R}^{\ell_y}$ ,  $u_t \in \mathbb{R}^{\ell_u}$ .  $A$ ,  $B$ ,  $C$  are known model matrices of appropriate dimensions;  $v_t$  and  $w_t$  are additive random processes expressing observational and modelling uncertainties, respectively, and their stochastic model must now be specified. We assume that  $v_t$  and  $w_t$  are mutually independent white noise processes uniformly distributed on *known* supports of finite measure:

$$f(v_t) = \mathcal{U}_v(-\nu, \nu), \quad f(w_t) = \mathcal{U}_w(-\omega, \omega), \quad (16)$$

where  $\omega \in \mathbb{R}^{\ell_x}$ ,  $\nu \in \mathbb{R}^{\ell_y}$ , with finite positive entries, and  $\mathcal{U}_\bullet$  denotes the uniform pdf on an orthotopic support (UOS), as now defined.

**Remark 1.** Consider a finite-dimensional vector random variable,  $z \in \mathbb{Z}_\mathbb{O}$ , with realisations in the following bounded subset of  $\mathbb{R}^{\ell_z}$ :

$$\mathbb{Z}_\mathbb{O} \equiv \{z : \underline{z} \leq z \leq \bar{z}\}, \quad \underline{z} < \bar{z} \quad (17)$$

where  $\underline{z}, \bar{z} \in \mathbb{R}^{\ell_z}$ . This convex polytope,  $\mathbb{Z}_\mathbb{O}$ , is called an orthotope.

The uniform pdf of  $z$  on the orthotopic support (17) called the UOS pdf is defined as

$$\mathcal{U}_z(\underline{z}, \bar{z}) \equiv \mathcal{V}_O^{-1} \chi_z(\underline{z} \leq z \leq \bar{z}), \quad (18)$$

where  $\mathcal{V}_O = \prod_{i=1}^{\ell_z} (\bar{z}_i - \underline{z}_i)$ .

Model (14), (15), (16), together with (18), defines the linear state-space mode with uniform additive noises on orthotopic supports, denote the LSU-UOS model. Its observation and state evolution models (1) are equivalently specified as

$$f(y_t|x_t) \equiv \mathcal{U}_y(\tilde{y}_t - \nu, \tilde{y}_t + \nu) \quad (19)$$

$$f(x_{t+1}|x_t, u_t) \equiv \mathcal{U}_x(\tilde{x}_{t+1} - \omega, \tilde{x}_{t+1} + \omega). \quad (20)$$

Exact Bayesian filtering for the LSU model (19) and (20)—i.e. computation of  $f(x_t|d(t))$  following (2) and (3)—is intractable, since the UOS class of pdfs (Remark 1) is not closed under those filtering operations. One consequence is that the dimension of the sufficient statistic of the filtering pdf (2) is unbounded as  $t$  grows i.e. at an infinite filtering horizon and so cannot be implemented (the curse of dimensionality [35]). In [41, 42], approximate Bayesian filtering with the LSU model (19) and (20), closed within the UOS class (18), is proposed. This involves a local approximation after each data update (2) and time update (3), as recalled below. This tractable but approximate Bayesian filtering procedure will be called *LSU-UOS Bayesian filtering*.

### 3.1.1. LSU-UOS data update

Define a *strip*,  $\mathbb{Z}_{\mathbb{S}}$ , as a set in  $\mathbb{R}^{\ell_z}$  bounded by two parallel hyperplanes, as follows:

$$\mathbb{Z}_{\mathbb{S}} = \{z : a \leq c' z \leq b\}. \quad (21)$$

Here  $a < b$  are scalars, and  $c \in \mathbb{R}^{\ell_z}$ .

In the data update (2), prior  $f(x_t|d(t-1)) = \mathcal{U}_x(\underline{x}_t^+, \bar{x}_t^+)$  is processed together with  $f(y_t|x_t)$  in (19), and with the latest observation,  $y_t$ , via Bayes' rule. It starts at  $t=1$  with  $f(x_1) = \mathcal{U}_x(\underline{x}_1^+, \bar{x}_1^+)$ . The resulting filtering pdf is uniformly distributed on a polytopical support that results from the intersection of the orthotopic support of  $f(x_t|d(t-1))$  and  $\ell_y$  strips induced by the latest observation,  $y_t$ :

$$\begin{aligned} f(x_t|d(t)) &\propto \mathcal{U}_x(\underline{x}_t^+, \bar{x}_t^+) \mathcal{U}_x(y_t - \nu \leq Cx_t \leq y_t + \nu) \propto \\ &\propto \chi_x \left( \begin{bmatrix} \underline{x}_t^+ \\ y_t - \nu \end{bmatrix} \leq \begin{bmatrix} I \\ C \end{bmatrix} x_t \leq \begin{bmatrix} \bar{x}_t^+ \\ y_t + \nu \end{bmatrix} \right). \end{aligned} \quad (22)$$

In [41], a local approximation is proposed so that the resulting polytopical support of (22) is circumscribed by an orthotope, giving

$$f(x_t|d(t)) \approx \mathcal{U}_{x_t}(\underline{x}_t, \bar{x}_t). \quad (23)$$

The approximate Bayesian sufficient statistics,  $\underline{x}_t$  and  $\bar{x}_t$ , process  $d(t)$  tractably  $\forall t$ , yielding an implementable algorithm. The details are provided in [41].

### 3.1.2. LSU-UOS time update

It now remains to ensure that each data update (above) is, indeed, presented with a UOS output from the preceding time update, as presumed. In each time update, the UOS posterior,  $f(x_t|d(t))$  (23), is processed together with  $f(x_{t+1}|x_t, u_t)$  (20)—uniform on  $\ell_x$   $x_t$ -dependent strips—via the marginalization operator in (3). The resulting pdf does have an orthotopic support, but is not uniform on it. In [41], the following local approximation projects  $f(x_{t+1}|d(t))$  back into the UOS class,  $\forall t$ :

$$f(x_{t+1}|d(t)) \approx \mathcal{U}_{x_{t+1}}(\underline{x}_{t+1}^+, \bar{x}_{t+1}^+) \quad (24)$$

where

$$\begin{aligned} \underline{x}_{i,t+1}^+ &= \sum_{j=1}^{\ell_x} \min\{A_{ij}\underline{x}_{t,j} + B_i u_t, A_{ij}\bar{x}_{t,j} + B_i u_t\} - \omega_i \\ \bar{x}_{i,t+1}^+ &= \sum_{j=1}^{\ell_x} \max\{A_{ij}\underline{x}_{t,j} + B_i u_t, A_{ij}\bar{x}_{t,j} + B_i u_t\} + \omega_i, \end{aligned} \quad (25)$$

$i = 1, \dots, \ell_x$ .

### 3.2. FPD-BTL between a pair of LSU-UOS filtering tasks

We now return to the central concern of this paper: the static FPD-optimal transfer of the state predictor,  $f_s(x_{s,t}|d_s(t-1))$ , from the source LSU-UOS filter (“the source task”) to the target LSU-UOS filter (“the target task”). The transfers will occur *statically*,  $\forall t \in \mathbb{T}$ , meaning that the *marginal* state predictor,  $f_s(x_{s,t}|d_s(t-1))$  is transferred in each step of FPD-BTL. (For a derivation of joint source knowledge transfer—i.e. dynamic transfer—in Kalman filters, see [43].)

Although there exists an explicit functional minimizer of (13) (see. [38]), our specific purpose here is to instantiate this FPD-optimal solution for UOS-closed filtering in the source and target tasks, as defined in Section 3.1.

We propose that the FPD-optimal target knowledge-constrained observation model (13) (i.e. after transfer),  $f^o \equiv f(y_t|x_t, f_s)$ , be uniform with its support,  $\check{\mathbb{Y}}_t|x_t$ , bounded (here, our set notation emphasizes the fact that the support is a function of  $x_t$ ). We now prove that this choice is closed under the FPD optimization (13). While the following theorem is formulated for uniform pdfs on *general* bounded sets, it is applied to our UOS class in the sequel.

**Theorem 1.** *Let the target’s ideal pdf in FPD (13) be its isolated joint predictor (10). Assume that the target’s (pre-transfer) state predictor,  $f(x_t|d(t-1))$  is uniform on bounded support,  $\mathbb{X}_t$ .  $f(y_t|x_t)$  is defined in (19). The transferred source state predictor,  $f_s(x_{s,t}|d_s(t-1))$ , is also uniform, with bounded support,  $\mathbb{X}_{s,t}$ . Define the bounded intersection (Figure 2):*

$$\mathbb{X}_t^\cap = \mathbb{X}_{s,t} \cap \mathbb{X}_t. \quad (26)$$

*Assume that the (unoptimized) variational target observation model,  $\check{f}(y_t|x_t, f_s)$  (11), is also uniform with bounded support.*

*If  $\mathbb{X}_t^\cap \neq \emptyset$ , then the optimal choice of  $\check{f}(y_t|x_t, f_s)$  minimizing the FPD objective (13) is*

$$f(y_t|x_t, f_s) \propto f(y_t|x_t \in \mathbb{X}_t^\cap) \quad (27)$$

*where the FPD-optimal set of  $x_t$  after transfer of the source knowledge is deduced to be  $\mathbb{X}_t^o = \mathbb{X}_t^\cap$ .*

*If  $\mathbb{X}_t^\cap = \emptyset$ —a testable condition before transfer—then knowledge transfer is stopped,<sup>1</sup> and  $f(y_t|x_t, f_s) \equiv f(y_t|x_t)$ , i.e. the optimal target conditional observation model is defined to be that of the isolated target.*

*Proof.* See Appendix A.1 □

The sets  $\mathbb{X}_t$  and  $\mathbb{X}_{s,t}$  are functions only of  $d(t-1)$  and  $d_s(t-1)$ , respectively, i.e. they are local *statistics* of the target or source tasks, respectively. In this way, FPD-BTL is effecting transfer of optimal statistics (knowledge) from source to target, in the spirit of knowledge fusion (Section 1). This is in contrast to any requirement to transfer raw data from the source, for processing in the target,

---

<sup>1</sup>This decision is consistent with the definition of conditional probability.

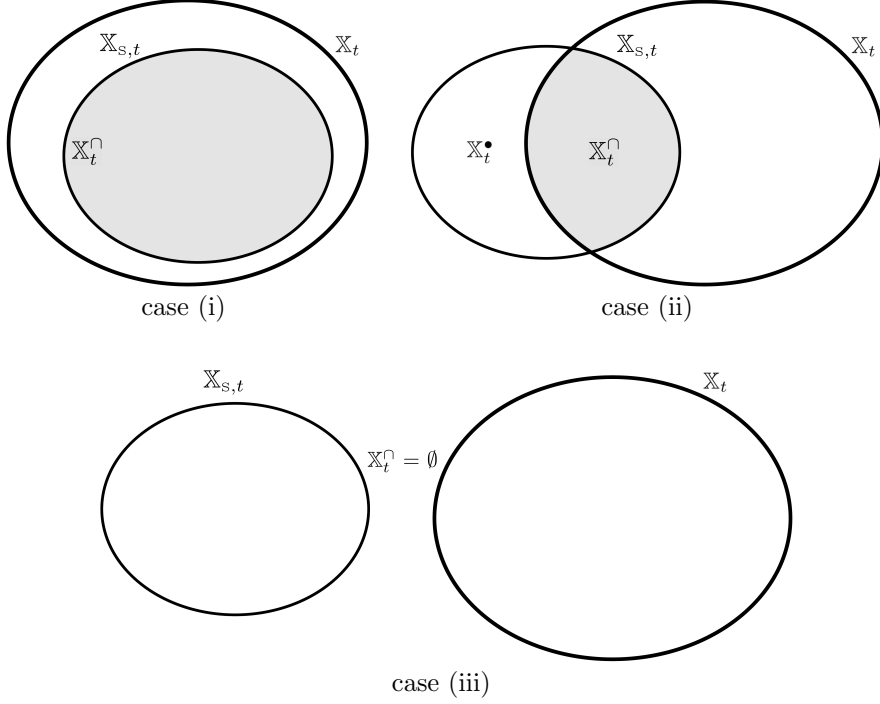


Figure 2: The mutual positions of the supports,  $\mathbb{X}_{S,t}$  of  $f_S(x_{S,t}|d_S(t-1))$ , and  $\mathbb{X}_t$  of  $f(x_t|d(t-1))$ . The cases (i), (ii) and (iii) are separately considered in the proof of Theorem 1.

as occurs in conventional multi-task inference (see Section 4). This property of transfer of source-optimal statistics to the target is a defining characteristic of FPD-BTL.

**Corollary 2** (Specialization to the UOS case). *Orthotopic sets (17) are closed under the intersection operator (26) (if  $\mathbb{X}_t^\cap \neq \emptyset$ ). Specifically, if  $\mathbb{X}_{S,t} = \{x : \underline{x}_{S,t} \leq x \leq \bar{x}_{S,t}\}$  and  $\mathbb{X}_t = \{x : \underline{x}_t \leq x \leq \bar{x}_t\}$ , then the FPD-optimal set of  $x_t$  after transfer (27) is*

$$\mathbb{X}_t^o = \mathbb{X}_t^\cap = \{x : \max(\underline{x}_{S,t}, \underline{x}_t) \leq x \leq \min(\bar{x}_{S,t}, \bar{x}_t)\}. \quad (28)$$

**Corollary 3.** (27) *constrains the allowed set of states in the target's subsequent (i.e. post-transfer) processing of local datum,  $d_t$ , via data update (2). The latter can be written as*

$$\begin{aligned} f(x_t|d(t), f_S) &\propto f(y_t|x_t, f_S) f(x_t|d(t-1)) \propto \\ &\propto f(y_t|x_t) \underbrace{f(x_t|d(t-1)) \chi(x_t \in \mathbb{X}_t^o)}_{\propto f(x_t|d(t-1), f_S)}. \end{aligned} \quad (29)$$

*Effectively, then the FPD-optimal transfer restricts the support of the target's (prior isolated) state predictor,  $f(x_t|d(t-1))$ , to  $\mathbb{X}_t^\cap$  (26), and this then forms the*

prior for the subsequent processing of the target’s local datum, via a conventional data update (29).

Additional notes:

- The knowledge is processed sequentially in the target, i.e. *firstly* the target processes local  $f_s(x_{s,t}|d_s(t-1))$ , yielding  $f(y_t|x_t, f_s)$ , (27); *secondly*, the target filter processes local  $y_t$  (data update (29)); *thirdly* the target predicts  $x_{t+1}$  via the *local* target time update (3), making available to the next (3-part) step of FPD-BTL its knowledge-conditional state predictor,  $f(x_{t+1}|d(y), f_s)$ . Knowledge transfer is therefore interleaved between the time and data updates.
- The FPD-optimal intersection (26), (27) is a concentration operator in the inference scheme (see Figure 2), ensuring entropy reduction and consistency properties [44] which—though evident—are not proven here.
- Recall the full acceptance of the source’s state predictor by the target, this induces a discontinuity between  $\mathbb{X}_t^\cap \neq \emptyset$  and  $\mathbb{X}_t^\cap \equiv \emptyset$  in Theorem 1 (see Figure 2). This artefact will be discussed further in Section 4.7.

The implied algorithmic sequence for FPD-BTL between a pair of LSU-UOS filters is provided in Algorithm 1.

### 3.3. FPD-BTL for multiple LSU-UOS sources and a single LSU-UOS target

Here, we extend FPD-BTL (Sec. 3.2) to the case of multiple bounded-support sources, which can be specified to the case of multiple interacting LSU-UOS tasks, again via Corollaries 2 and 3. Assume the same scenario as in Figure 1, with one target but, now,  $n - 1$  sources,  $n \geq 2$  (i.e.  $n \geq 2$  interacting LSU-UOS tasks in total). Once again, the instantiation of the  $n$  tasks is avoided (i.e. incomplete modelling). Each source provides its state predictor  $f_{s_i}(x_{s_i,t}|d_{s_i}(t-1))$ ,  $i = 1, \dots, n - 1$ , statically,  $\forall t$ , to the target in the same way as in the single source setting.

**Theorem 4.** *Let there be  $n \geq 2$  state-space filters,  $f_1, f_2, \dots, f_n$ , having bounded supports of their state predictors,  $\mathbb{X}_{1,t}, \mathbb{X}_{2,t}, \dots, \mathbb{X}_{n,t}$ , respectively. Assume  $f_1$  is the target filter, and  $f_2, \dots, f_n$  the source filters. Then the FPD-optimal target observation model after transfer for the  $n - 1$  source state predictors is*

$$f(y_t|x_t, f_2, \dots, f_n) = f(y_t|x_t \in \mathbb{X}_t^o),$$

where

$$\mathbb{X}_t^o = \bigcap_{k=1}^n \mathbb{X}_{k,t}. \quad (30)$$

*Proof.* See Appendix A.2. □

---

**Algorithm 1:** FPD-BTL between two LSU-UOS filtering tasks

---

**Initialization:**

- set the initial time  $t = 1$  and the final time  $\bar{t} > 1$
- set prior values  $\underline{x}_1^+, \bar{x}_1^+$  for  $f(x_1|d(0)) \equiv f(x_1) = \mathcal{U}_x(\underline{x}_1^+, \bar{x}_1^+)$
- set  $f(x_{s,1}|d_s(0)) \equiv f_s(x_{s,1}) = \mathcal{U}_s(\underline{x}_{s,1}^+, \bar{x}_{s,1}^+)$
- set noise bounds  $\nu, \omega$  (16)

**Recursion: for  $t = 1, \dots, \bar{t} - 1$  do**I. *Knowledge transfer:*

transfer orthotopic  $f_s(x_{s,t}|d_s(t-1))$  (6)  
and compute  $f(x_t|d(t-1), f_s)$  (29) via (26) and (28)

II. *Data update:*

process local target datum,  $d_t$ , into  $f(x_t|d(t))$  (23) via orthotopic approximation of (22), specified in [41]

III. *Time update:*

compute  $f(x_{t+1}|d(t)) = \mathcal{U}_x(\underline{x}_{t+1}^+, \bar{x}_{t+1}^+)$  (24) via (25)

**end****Termination:** set  $t = \bar{t}$ I. *Knowledge transfer:*

transfer final orthotopic  $f_s(x_{s,\bar{t}}|d_s(\bar{t}-1))$  (6)  
and compute  $f(x_{\bar{t}}|d(\bar{t}-1), f_s)$  (29) via (26) and (28)

II. *Data update:*

process final local target datum,  $d_{\bar{t}}$ , into  $f(x_{\bar{t}}|d(\bar{t}))$  (23) via orthotopic approximation of (22) [41]

---

## 4. Simulations studies

In this section, we provide a detailed study of the performance of the proposed Bayesian transfer learning algorithm (FPD-BTL) between LSU-UOS filtering tasks. We compare it to Bayesian complete (network) modelling (BCM, to be defined below) for the UOS class and to the distributed set-membership fusion algorithm (DSMF) for ellipsoidal sets [24], which also involves complete modelling of the networked LSU filters.

In the design of these comparative experiments, our principal concerns are the following:

1. To study the influence of the number of sources on the performance of the target filter in FPD-BTL (experiment #1).
2. To compare FPD-BTL to complete modelling alternatives (BCM and DSMF, experiment #2).
3. To study the robustness of FPD-BTL—which does not require for tasks interaction (i.e. it is incompletely modelled)—to model mismatches that inevitably occur between source and target tasks in the complete modelling approaches (BCM and DSMF) (experiments #3–#5).
4. To assess the computational demands of the proposed FPD-BTL algorithm in comparison to the competitive methods (BCM and DSMF).

Section 4.1 explains the necessary background, emphasizing the important distinction between the *synthetic* and *analytic* model in these simulation studies. Then, model mismatch and its types are specified (Sections 4.1.1 and 4.1.2). The specific LSU-UOS systems (19), (20) used in our studies are described in Section 4.2. The completely modelled alternatives (BCM and DSMF) are reviewed in Section 4.3, and the evaluation criteria are defined in Section 4.4. Then, the experimental results are presented and discussed in Section 4.5, before overall findings are collected and interpreted in Section 4.7.

### 4.1. Synthetic vs. analytic models

In computer-based simulations—such as those which follow—we explicitly distinguish between the *synthetic* model, used for data generation, and the *analytic* model on which the derived state estimation algorithm depends. The synthetic model can be understood as an abstraction of a natural (physical) data-generating process, while the analytic model is a subjective (i.e. epistemic [45])—and inevitably *approximate*—description of this process adopted by the inference task (here, the LSU-UOS filters).

Figure 3 shows three models for a pair of state-space filters adopted in this paper, as either synthetic or analytic models (or both). If the V-shaped graph (Figure 3a) is used as the synthetic model, state sequence  $\{x_t\}_{t=1}^{\bar{t}}$  is realized commonly for all the filters, via the Markov state process (15), and then locally

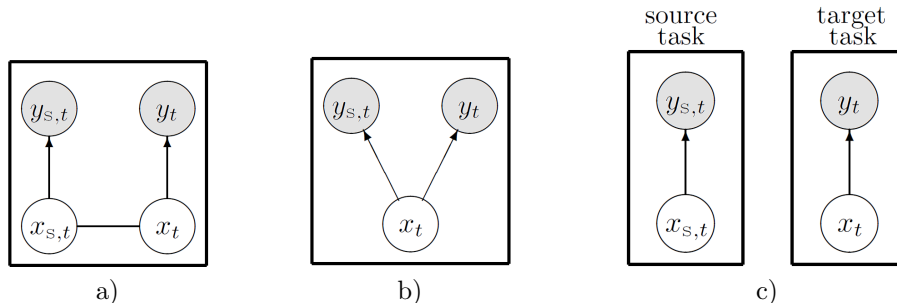


Figure 3: Models (synthetic and/or analytic) for a pair of state-space observation processes,  $y_{s,t}$  and  $y_t$ . a) V-shaped graph, single modeller; b) U-shaped graph, single modeller; c) multiple modellers. A frame denotes a modeller, that observes data (shaded nodes), and for which stochastic dependencies within the frame are known. Conditional and joint probability models of these dependencies are represented by arrows and by lines (i.e. undirected and directed edges), respectively, as usual [46]. The schemes show the marginal relationship between states and observations within one filtering step of dynamic modelling, but not the (temporal) dynamics themselves.

corrupted via independent, additive, white UOS observation noise processes  $v_{k,t}$  (14). If the analytic model is also the V-shaped graph (Figure 3a) with *known* parameters, then we refer to this as complete modelling, as adopted in BCM and DSMF.

The U-shaped graph (Figure 3b) is adopted as the synthetic model in some of the experiments below. here, the target state sequence,  $\{x_t\}_{t=1}^{\bar{t}}$  and source state sequence  $\{x_{s,t}\}_{t=1}^{\bar{t}}$  are synthesized as distinct—but mutually correlated—processes, with an appropriate fully specified interaction model between  $x_t$  and  $x_{s,t}$ . The U-shaped graph is not used as an analytic model in this paper.

As already explained in sections 2 and 3, the multiple modeller approach (Figure 3c) is adopted as the analytic model only in our proposed FPD-BTL approach, expressing the fact that the target elicits no model of the source process or of its relationship to it. The source and target analytic models are therefore stochastically independent, and can be interpreted as independent 2-node marginals of a (unspecified) 4-node complete model. This arrangement respects the key notion of *local expertise*, i.e. the commonly encountered situation in distributed inference where the source is a better local analytic modeller (i.e. expert) of its local data than the remote target modeller ever can be.

In the simulation studies most frequently encountered in the literature, the synthetic and analytic models are implicitly assumed to be identical. In the computer-based synthetic-data experiments below, *modelling mismatch* can be explored, and is, indeed, our priority. However, in real-data studies, the notion of a synthetic model is inadmissible [45]. It follows that there is therefore almost-sure mismatch between the (typically unknowable) “truth theory” of synthesis [45] and the analysis model which prescribes the adopted algorithm. It is for this reason that a study of analysis-synthesis modelling mismatch—as provided below—is of key importance, particularly in assessment of the robust-

ness or fragility of the algorithm to such mismatches.

In the forthcoming simulations, modelling mismatch will be arranged at the level of the state sequence(s), either via mismatches in the process noise  $w_t$  (16), or state matrix mismatches,  $A$  (15). These are detailed in the next two subsections.

#### 4.1.1. State noise mismatch

The target filter's state at time  $t$  is synthesized according to (15) with a uniform noise,  $w_t$  (16). If the sequence  $\{x_t\}_{t=1}^{\bar{t}}$  is common for both the filters, data synthesis is described by the V-shaped graph (Figure 3a), as already noted in Section 4.1. Synthesis via the U-shaped graph (Figure 3b) realizes distinct state processes,  $x_t$  and  $x_{s,t}$ , via the operating parameter,  $\alpha \geq 0$ , which controls the interaction (i.e. correlation) between them:

$$\begin{aligned} x_{s,t} &= Ax_{s,t-1} + Bu_{s,t-1} + w_{s,t}, & w_{s,t} &\sim \mathcal{U}(-\omega, \omega), \\ x_t &= x_{s,t} + e_t, & e_t &\sim \mathcal{U}(-\alpha\omega, \alpha\omega). \end{aligned} \quad (31)$$

Here,  $w_t$  and  $e_t$  are mutually independent, white UOS state processes in  $\mathbb{R}^{\ell_x}$ . The source's analytic model is also given by (15) with perfectly matched parameters. However, we will assume that the target modeller is *unaware* of the mismatching noise process,  $e_t$ , and so the target's analytic model of their local state process,  $x_t$ , is also (15). This enforces a mismatch between the target's synthetic model (31), and its analysis model (15), via the state noise mismatch process,  $e_t$  (31). Note that if  $\alpha = 0$ , the source and target synthesized states are identical (Figure 3a) and matched to the source and target analysis models(s). In contrast, if  $\alpha > 0$ , then the marginal synthesis model (i.e. pdf) of  $x_t$  is trapezoidal (being the convolution of two uniform pdfs) with increased variance, while the target's mismatched local analytic state model is uniform (20).

#### 4.1.2. State matrix mismatch in the analytic models

In this section, we distinguish between the state matrix (15) in synthesis,  $A^{(s)}$ , of the common state process,  $x_t$ , (Figure 3a), and the state matrix/matrices used in analysis,  $A^{(a)}$ . Specifically, we set  $A_s^{(a)} = A^{(s)}$  (i.e. no synthesis-analysis mismatch in the source), but  $A^{(a)} \neq A^{(s)}$  (i.e. mismatch in the target). There are several ways to achieve  $A^{(a)} \neq A^{(s)}$ :

1. Modification of the eigenvalues of invertible  $A^{(s)} = V^{(s)}\Lambda^{(s)}V^{(s)-1}$ . In the target analytic model, we modify the eigenvalues of  $A^{(a)}$  geometrically in one of two ways:
  - (a) Radial shift: a selected eigenvalue  $\lambda_i^{(s)}$ ,  $i \in \{1, \dots, \ell_x\}$  of  $A^{(s)}$  is multiplied by a real scalar operating parameter  $q > 0$ , i.e.  $\lambda_i^{(a)} \equiv q\lambda_i^{(s)}$ , while maintaining Hermitian symmetry.
  - (b) Rotation: here,  $\lambda_i^{(s)}$  is multiplied by a factor,  $e^{j\varphi}$ , where the angle of rotation,  $\varphi$ , is the operating parameter, i.e.  $\lambda_i^{(a)} \equiv e^{j\varphi}\lambda_i^{(s)}$ . Once again, Hermitian symmetry is maintained.

2. Multiplication of  $A^{(s)}$  by a scalar,  $\sigma > 0$ , i.e.  $A^{(a)} \equiv \sigma A^{(s)}$ . In this case, all eigenvalues of  $A^{(s)}$  experience the same radial shift.

#### 4.2. The synthesis models

The following specific LSU systems (14), (15), are simulated in the upcoming experiments, i.e. they specify the synthesis model for both  $y_{s,t}$  and  $y_t$  in the V-shaped graph (Figure 3a) or in the U-shaped graph (Figure 3b), as specified in (31). The uncertainty parameters,  $\nu$  and  $\omega$  (16), are specified in each experiment.

- A second-order system with two complex conjugate poles, described by (14) and (15), with  $\ell_x = 2$ ,  $\ell_u = 1$ ,  $\ell_y = 1$ , and

$$A = \begin{bmatrix} 0.8144 & -0.0905 \\ 0.0905 & 0.9953 \end{bmatrix}, \quad B = \begin{bmatrix} 0.0905 \\ 0.0047 \end{bmatrix}, \quad C = [0 \quad 1]. \quad (32)$$

This system is studied in [47], being the discretization and randomization of the continuous-time system,  $\ddot{y}(\tau) + 2\dot{y}(\tau) + y(\tau) = u(\tau)$ , with sampling period,  $T_0 = 0.1$  s, and with added random processes,  $v_t$  and  $w_t$ , representing observational and modelling (i.e. state) uncertainties, respectively.

- A third-order system with 3 distinct real poles, described by (14) and (15) with  $\ell_x = 3$ ,  $\ell_u = 1$ ,  $\ell_y = 2$ , and

$$A = \begin{bmatrix} 0.4 & -0.3 & 0.1 \\ -0.4 & 0.4 & 0 \\ 0.3 & 0.2 & 0.1 \end{bmatrix}, \quad B = \begin{bmatrix} 0.1 \\ 0.6 \\ 0.3 \end{bmatrix}, \quad C = \begin{bmatrix} 1 & 0 & 0.5 \\ 0 & 1 & 0.5 \end{bmatrix}. \quad (33)$$

#### 4.3. Alternative multivariate inference algorithms

The key distinguishing attribute of our FPD-BTL algorithm is its multiple modeller approach with incomplete modelling of the interaction between the tasks. Its defining characteristic—the transfer of source sufficient statistics and not raw data—for processing at the target, distinguishes it from methods that adopt a complete model of the networked tasks, often involving joint processing—at the target or other fusion centre—of the multiple raw data channels. We will reserve the term transfer learning (TL) for the former (FPD-BTL in the case of our FPD-optimal Bayesian TL scheme), and refer to the latter as multivariate inference schemes. We will compare FPD-BTL against two approaches to the latter: (i) Bayesian multivariate inference (Section 4.3.1) consistent with a complete analysis model (i.e. V-shaped network graph in Figure 3a); and (ii) distributed set-membership fusion (DSMF) (Section 4.3.2), a state-of-the-art, non-probabilistic, fusion-based state estimation algorithm [24].

#### 4.3.1. Bayesian complete modelling (BCM)

Here, it is assumed that the  $n$  LSU filters, indexed by  $i = 1, \dots, n$ , consist of  $n$  conditionally independent observation models with common Markov state evolution model (15) (i.e. the V-shaped graph as analytic model, Figure 3a). The  $n$  observation models are

$$y_{i,t} = C_i x_t + v_{i,t}, \quad i = 1, \dots, n, \quad (34)$$

where the known  $C_i \equiv C$  are possibly common, too, and the  $n$  UOS white noise channels are mutually independent. The filters are modelled by a central modeller with knowledge in all the parameters and data, i.e. the inference algorithm processes all  $n$  data channels,  $y_{i,t}$ .

The data update (2) uses the joint pdf of the  $n$  data channels to process  $y_{1t}, \dots, y_{nt}$  (of possibly different dimensions):

$$f(x_t | d_1(t), \dots, d_n(t)) \propto f(x_t | d_1(t-1), \dots, d_n(t-1)) \prod_{i=1}^n f(y_{i,t} | x_t), \quad (35)$$

initialized (at  $t = 1$ ) with the prior,  $f(x_1 | d_1(0), \dots, d_n(0)) \equiv f(x_1)$ .

The time update (3) is

$$f(x_{t+1} | d_1(t), \dots, d_n(t)) = \int_{\mathbb{X}_t} f(x_{t+1} | u_t, x_t) f(x_t | d_1(t), \dots, d_n(t)) dx_t. \quad (36)$$

The algorithmic solution of BCM, closed within the LSU-UOS class—i.e. with  $n + 1$  projections into the UOS class, per step of multivariate Bayesian filtering, as explained in Section 3.1—is straightforward, because all the pdfs have the same parametric form as in the single-output ( $n = 1$ ) case. In (35), the  $n$  data updates are computed by (22) and (23)—with arbitrary order—for each  $f(y_{i,t} | x_t)$  in turn. Then, the LSU-closed approximate time update is implemented via (36), in the usual way (Section 3.1.2).

#### 4.3.2. Distributed set-membership fusion (DSMF)

The DSMF estimation task for a multi-sensor dynamic system with unknown but bounded noises is presented in [24]. The state-space model (15) and (34) is driven by (unmodelled) noises conditioned to the following ellipsoidal sets:

$$\begin{aligned} \mathbb{V}_{i,t} &= \{v_{i,t} : v_{i,t}' R_{i,t}^{-1} v_{i,t} \leq 1\}, & i = 1, \dots, n, \\ \mathbb{W}_t &= \{w_t : w_t' Q_t^{-1} w_t \leq 1\}. \end{aligned} \quad (37)$$

Here, matrices  $R_{i,t}$  and  $Q_t$  are symmetric and positive definite of appropriate dimensions. The ellipsoids' centres are at the origin, enforcing a prior assumption of zero (time-averaged) mean noises.

While, the method is non-probabilistic, it adopts complete modelling via the V-shaped (analytic) graph (Figure 3a), with the edges defined only via geometric relationships. The resulting recursive algorithm consists of a deterministic

time update of the combined state estimate from the previous step, then a data update for each filter, and finally a fusion step, when individual state estimates are combined, using also the time-updated state. Optimal fusion weights are calculated by solving a convex optimization problem in each step of the algorithm.

#### 4.4. Evaluation criteria

For competitive quantitative evaluation of FPD-BTL, BCM and DSMF, we define the following performance quantities:

- Total norm squared-error (TNSE) of the state estimate:

$$\text{TNSE} = \sum_{t=\underline{t}}^{\bar{t}} \|\hat{x}_t - x_t\|_2^2, \quad (38)$$

$\underline{t} = 1$  for FPD-BTL and BCM, but is set higher—typically  $t/2$ —in DSMF, as explained later.  $\|\cdot\|_2$  is the Euclidean norm. In the FPD-BTL and BCM,  $\hat{x}_t$  is mean value of the UOS filtering pdf (23), either via (29) (i.e. line 2 of Algorithm 1), or via (35). In DSMF,  $\hat{x}_t$  is centre of the state’s estimated ellipsoid.

- Average posterior volume (AV). Define sequential  $\mathbb{X}_t \equiv \text{supp}(f(x_t|d(t), f_s))$  in the case of FPD-BTL (29), and  $\mathbb{X}_t \equiv \text{supp}(f(x_t|d(t), d_s(t)))$  in the case of BCM (35) (both orthotopic),  $\mathbb{X}_t \equiv \{x_t : x_t' P_t^{-1} x_t \leq 1\}$  (ellipsoidal) in the case of DSMF, where  $P_t$  is a sequentially computed matrix defining the bounding ellipsoid of  $\mathbb{X}_t$ . Let the Lebesgue measure (hypervolume) of  $\mathbb{X}_t$  be  $V_t = \mu(\mathbb{X}_t)$  in each case. Then

$$\text{AV} = \frac{1}{\bar{t} - \underline{t} + 1} \sum_{t=\underline{t}}^{\bar{t}} V_t. \quad (39)$$

- Average volume ratio (AVR). Let  $\mathbb{X}_t$  be defined as for the AV above, respectively. Let  $\text{VI}_t$  denote the Lebesgue measure of  $\mathbb{X}_t$  in the case of the isolated target (Figure 3c) (or without fusion, in the case of DSMF) and  $\text{VT}_t$  the same respective quantity with transfer/fusion. Then

$$\text{AVR} = \frac{1}{\bar{t} - \underline{t} + 1} \sum_{t=\underline{t}}^{\bar{t}} \frac{\text{VT}_t}{\text{VI}_t}. \quad (40)$$

It is an average ratio of concentration of the state inference under transfer fusion

- Containment probability ( $p_c$ ): this is the probability that the simulated—i.e. “true”—state  $x_t$  is contained in the respective inferred  $\mathbb{X}_t$ , as defined

for AV above. This probability is calculated as a relative frequency of containment occurrence:

$$p_c = \frac{1}{\bar{t} - \underline{t} + 1} \sum_{t=\underline{t}}^{\bar{t}} \chi(x_t \in \mathbb{X}_t). \quad (41)$$

- Computation time for comparison of FPD-BTL with DSFM by multiple executions with various noise parameters, run on PC Matlab.

In the experiments below, the vector noise parameters,  $\nu \in \mathbb{R}^{\ell_y}$  and  $\omega \in \mathbb{R}^{\ell_x}$  (16), are isotopic, i.e.

$$\nu = r \mathbf{1}_{(\ell_y)}, \quad \omega = \rho \mathbf{1}_{(\ell_x)}, \quad (42)$$

where  $\rho$  and  $r$  are positive scalars and  $\mathbf{1}_{(k)}$  is the  $k$ -dimensional unit vector.

The figures below graph the dependence of TNSE (38), average volume (AV) (39) and average volume ratio (AVR) (40) against the source-to-target ratio of the observation noise variances, i.e.  $r_s/r$ . For all these performance quantities, smaller is better. Conversely, the containment probability,  $p_c$  (41), where evaluable, is a bigger is better quantity. Because of their wide numerical ranges, the quantities (38), (39) and (40) are plotted logarithmically. They are also evaluated for the (isolated)  $y_t$  channel in each case (Figure 3) providing a benchmark (i.e. datum) against which to assess the impact of the various  $y_s$ -processing algorithms. FPD-BTL and BCM will be identical in this isolated  $y_t$  case. In these non- $d_{s,t}$  cases, performance is of course invariant with  $r_s/r$ .

For each setting of  $r_s/r$ , the performance graphs are obtained as the average over MC=50 or 500 Monte Carlo runs, holding all the synthetic model parameters ( $A, B, C, \rho, r$ ) constant (14), (15), (42).

In the case of  $n = 2$  data channels, the operating parameter,  $r_s/r = 1$ , constitutes a *threshold*. If  $r_s/r < 1$  (which we call the above-threshold region),  $y_{s,t}$  reduces uncertainty in  $x_t$  in our FPD-BTL algorithm, as we will see. We call this *positive transfer* (i.e. improved performance relative to the isolated target task). Conversely, if  $r_s/r > 1$  (below threshold),  $y_{s,t}$  may undermine the estimation of  $x_t$ , depending on the algorithm. To be *robust*, state estimation performance should revert to estimation conditioned only on  $y_t$  (i.e. the algorithm should be capable of rejecting knowledge from  $y_s$ ). A key priority of our studies below will be to assess how robust our FPD-BTL algorithm is in comparison with the alternatives.

#### 4.5. Experimental results

The modelling choices of the experiments are summarized in Table 1. Each row refers to a particular experiment (#1–#5) to follow. Columns record which synthetic model—a or b in Figure 3—is used to simulate the data, and which—a or c—is adopted as the analytic model in the respective algorithm (FPD-BTL, BCM and DSFM). The last column indicates whether the state synthesis and (target) analysis matrices,  $A^{(s)}$  and  $A^{(a)}$  respectively, are set equal or not (see Section 4.1.2).

experiment	synthetic	BTL analytic	BGM analytic	DSMF analytic	$A^{(s)} \equiv A^{(a)}$
#1 (Sec. 4.5.1)	a	c	—	—	✓
#2 (Sec. 4.5.2)	a	c	a	a	✓
#3 (Sec. 4.5.3)	a	c	a	a	×
#4 (Sec. 4.5.3)	a	c	a	a	×
#5 (Sec. 4.5.3)	b	c	a	a	✓

Table 1: The synthetic and analytic models adopted in each experiment. Symbols a, b, c refer to the graphical models in Figure 3.

#### 4.5.1. FPD-BTL with multiple source tasks

Experiment #1: Here, the performance of an isolated target LSU-UOS filter is compared to FPD-BTL with multiple source filters. State synthesis model (32) is adopted with state sequence,  $x_t$ , noisily observed in each of  $n$  scalar i.i.d. data channels,  $n = 2, 11, 101, 1001$  (i.e. for  $n_s = n - 1 = 1, 10, 100, 1000$  source tasks, respectively, plus 1 target task). In all settings,  $\rho = 10^{-5}$ ,  $r = 10^{-3}$  (42),  $\underline{t} = 1$ ,  $\bar{t} = 50$ , MC = 500 runs. Performances are evaluated via TNSE (38) and AVR (40), in comparison to the isolated target filter. We observe the following:

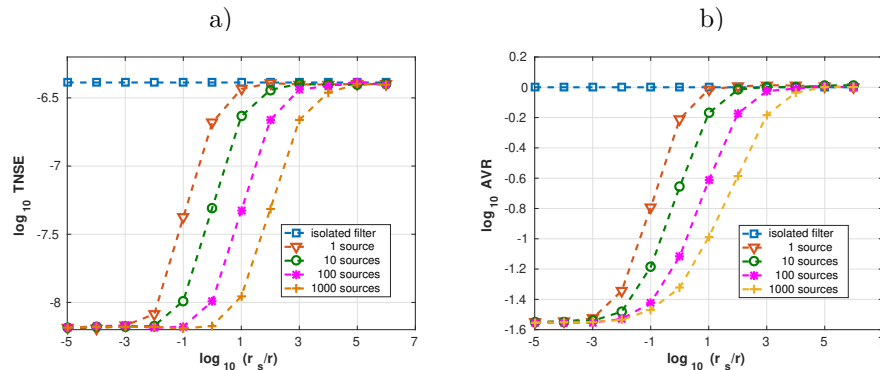


Figure 4: Experiment #1: Comparison of isolated target filtering task and FPD-BTL with multiple source filtering tasks. a) TNSE (38) and b) AVR (40), system (32), various numbers of source tasks.

- (i) FPD-BTL exhibits *positive transfer* above threshold; i.e. the transferred source knowledge improves the performance of the target.
- (ii) FPD-BTL is *robust*; i.e. the target becomes isolated from the sources (transfer is quenched) in cases of poor-quality source knowledge (below threshold, where the source state-predictive variance is high relative to that of the isolated target). In this way, *negative transfer*—a hazard of transfer learning algorithms [39], [23]—is eliminated.
- (iii) The  $r_s/r$  threshold increases monotonically with the number of sources.

For  $n_s=1$ , the threshold is  $r_s \approx 10r$ . However, poor-quality sources continue to deliver positive transfer to the target up to a threshold,  $r_s = 10n_s r$ , in the multi-source case. The threshold is found to be independent of  $\bar{t}$ .

- (iv) All performances saturate in very positive transfer regimes (i.e. where  $r_s \ll r$ ). The bound is determined by  $\rho$  and  $r$  (42), which are invariant.

The containment probability,  $p_c$  (41), is identically 1 for all the runs, i.e. all the “true” (simulated) states are contained in the posterior LSU-UOS support.

#### 4.5.2. Comparison of FPD-BTL, BCM and DSMF for $n = 2$ data channels

Experiment #2: In all forthcoming experiments,  $n = 2$ , i.e. 2 data channels, with the single LSU-UOS source task ( $n_s = 1$ ) processing  $d_{s,t}$  and the single target task processing  $d_t$  in FPD-BTL. The fully modelled alternatives (BCM and DSMF) process  $d_{s,t}$  and  $d_t$  together. In the current experiment (#2), common state process,  $x_t \in \mathbb{R}^2$ , is synthesized via system (32) with  $\rho = 10^{-5}$ , and  $r = 10^{-3}$  in the  $n = 2$  conditionally iid data channels,  $\underline{t} = 2000$ ,  $\bar{t} = 4000$  and MC = 50 runs.

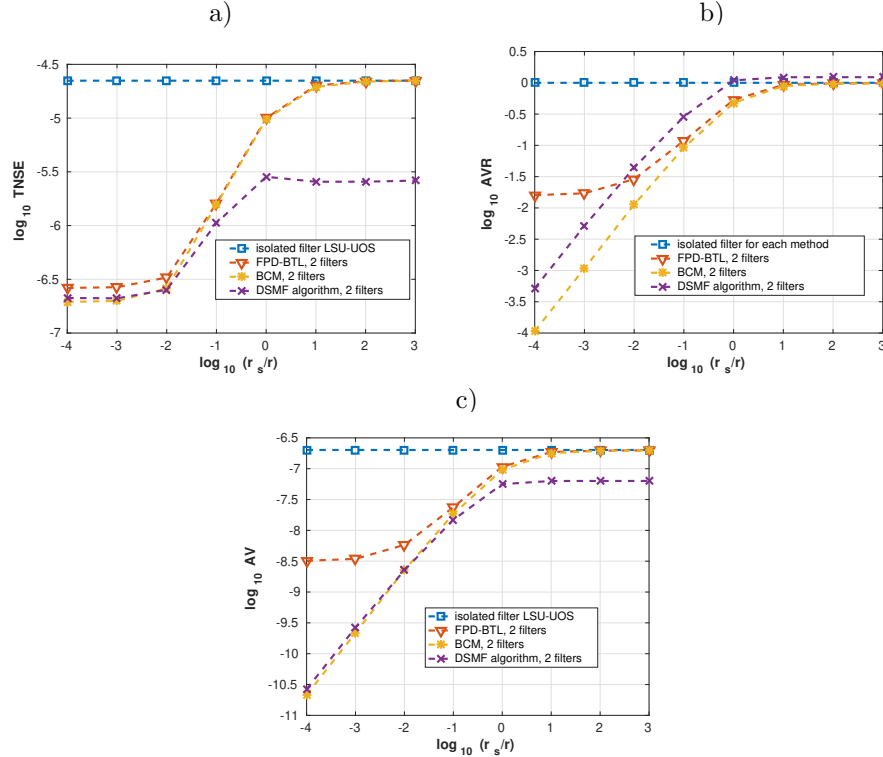


Figure 5: Experiment #2: Filtering performance of FPD-BTL compared to the isolated LSU-UOS task (32), and to complete modelling alternatives (BCM and DSMF): a) TNSE (38), b) AVR (40) and c) AV (39).

The performance of the isolated target task (processing  $d_t$  alone) is compared to our FPD-optimal BTL scheme and to the joint processing alternatives under three performance criteria (Figure 5). All the characteristics are decreasing as  $r_s$  decreases. We note the following:

- (i) The threshold for FPD-BTL and BCM is  $\log_{10} r_s/r = 1$ , in agreement with experiment #1. The threshold for DSMF is  $\log_{10} r_s/r = 0$ .
- (ii) Below threshold ( $\log_{10} r_s/r > 1$ ), the absolute performance quantities (TNSE (38), Figure 5a, and AV (39), Figure 5c) coincide for the Bayesian LSU-UOS methods (FPD-BTL and BCM); the DSMF shows better performance.
- (iii) Above threshold ( $\log_{10} r_s/r < 1$ ), the characteristics mentioned above coincide for complete modelling methods (BCM and DSMF), outperforming FPD-BTL.
- (iv) Since the analytic and synthetic models match in the complete modelling approaches (BCM and DSMF), they provide better estimation than FPD-BTL, and DSMF dominates over BCM due to its tighter geometric approximation, although with a lower threshold.

Finally, we comment on the containment probability,  $p_c$  (not shown in Figure 5), i.e. the probability that the “true” (simulated) state is contained in the inferred  $\mathbb{X}_t$ , respectively (see the second bullet of Section 4.4). For the Bayesian LSU-UOS approaches *and if* the analytic and synthetic models match,  $p_c = 1$ . For DSMF,  $p_c < 1$  in many operating settings, depending on the system, noise, length of the burn-in period etc., however, very close to 1. This suggests that the containing ellipsoid in DSMF is estimated too small or mis-centered, missing the true state occasionally.

Experiment #2 was repeated with the system (33), providing very similar findings. However, above threshold,  $p_c$  for DSMF decreases to about 0.91.

#### 4.5.3. Modelling mismatch

In the remaining three experiments (#3–#5, see Table 1), our aim is to explore the freedom that derives from the fact that FPD-BTL is a multiple modeller framework, allowing the source modeller to adopt an analytic model different from the target’s (in all these experiments, we focus on  $n_s = 1$  source modeller).

In particular, we explore the additivity that arises from the case—often encountered in practical distributed inference and multisensor settings—where the source is an *expert*, meaning that the analytic model for its (local) source data,  $d_{s,t}$ , matches the synthetic model for  $d_{s,t}$  better than the analysis-synthesis arrangement for  $d_t$  in the target task (Figure 3c). Our experiments will focus on the case where the target’s analysis model for  $d_t$  is mismatched with respect to its synthesis model, while no such mismatch exists for the (expert) source’s data,  $d_{s,t}$ . The hypothesis we seek to test is that positive transfer from the

source’s matched state predictor,  $f(x_{s,t}|d_s(t-1))$  (24), can improve the target’s filtering performance, relative to complete modelling approaches—BCM and DSMF (Section 4.3)—where mismatching occurs in *both* channels,  $d_{s,t}$  and  $d_t$ .

*Experiment #3: Rotation of a pair of eigenvalues of  $A^{(s)}$ .* In the system (32), the state transition matrix in the synthesis model,  $A^{(s)}$ , has a pair of complex conjugate eigenvalues  $0.9049 \pm 0.003i$ . These eigenvalues are rotated (mismatched) by angle  $\pm\varphi$  (radians, preserving conjugacy), in the target’s analysis model (FPD-BTL), and in the completely modelled approaches (BCM, DSMF). The interval,  $\varphi \in (-0.007, 0.067)$ , represents the range (found experimentally) when  $\mathbb{X}_t^\cap \neq \emptyset$  in Theorem 1, and the estimation is numerically stable, i.e. the intersection in (22) is nonempty. To repeat: the data are synthesized with  $\varphi = 0$ ,

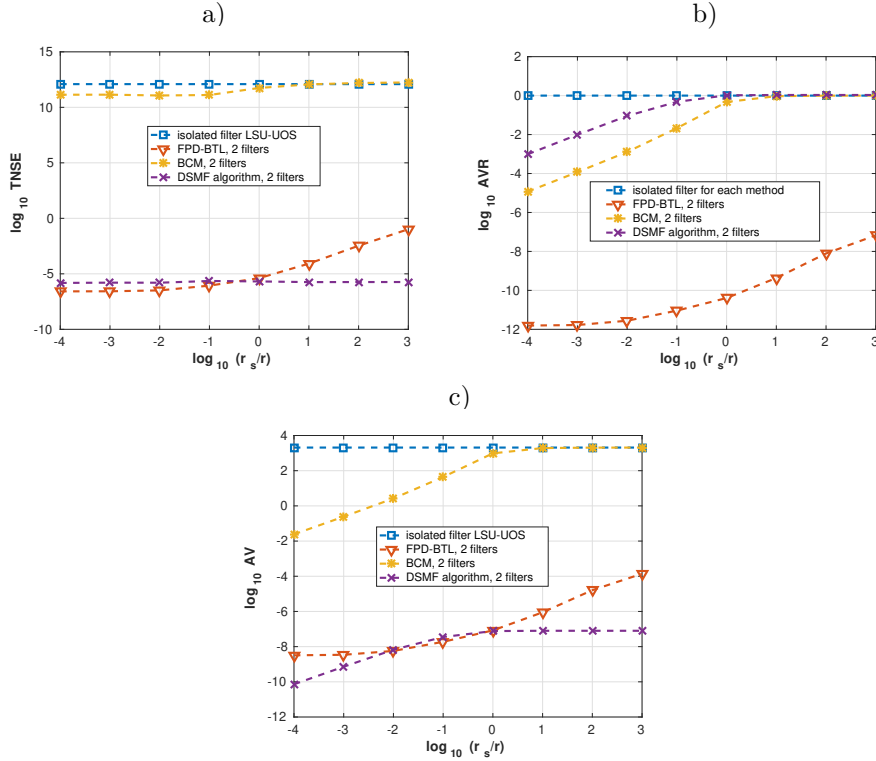


Figure 6: Experiment #3: a) TNSE (38), b) AVR (40) and c) AV (39), rotational mismatch— $\varphi = 0.067$ —of the eigenvalues of  $A$  (32) in the target’s analysis model (FPD-BTL), and in the complete analysis models (BCM and DSMF, V-shaped complete model (Figure 3a)).

i.e. with the  $A^{(s)} = A$  in (32), according to the V-shaped graph (Figure 3a). The same matrix,  $A^{(a)} = A$ , is used for the source analytic model. For the target analytic model,  $A$  is perturbed with  $\varphi = 0.067$ . This bounding value of  $\varphi$  in the interval above is adopted in order to illustrate relative algorithmic performance

under significant analysis-synthesis mismatch. Also,  $r = 10^{-3}$ ,  $\rho = 10^{-5}$  (42),  $\underline{t} = 2000$ ,  $\bar{t} = 4000$ , MC = 50 runs (Figure 6). We note the following:

- (i) The TNSEs for the (mismatched) isolated target filter and BCM are very high (Figure 6a), whereas the TNSE for FPD-BTL preserves the same positive transfer characteristic as was achieved with the matched target case (i.e.  $\varphi = 0$ , see Figure 5a).
- (ii) AV for FPD-BTL (Figure 6c) also preserves the same positive transfer characteristic as for  $\varphi = 0$ , outperforming BCM.
- (iii) DSMF is robust to this kind of modelling mismatch: its AV achieves values close to the matched ( $\varphi = 0$ ) case (Figure 5a). The TNSE of DSMF deteriorates insignificantly relative to the matched case, and is almost constant with  $r_s/r$ . In this experiment, DSMF outperforms the other methods.
- (iv) The  $r_s/r$  thresholds for BCM and DFSM are preserved.
- (v) FPD-BTL and DSMF are robust to  $r_s \gg r$ , in the sense that they achieve very low TNSE in this regime, both in absolute terms *and* relative to the mismatched isolated target.

Note that when  $\varphi$  is varied from 0 (matching) to 0.067 (maximal computationally stable mismatch), the performance measures (TNSE, AVR, AV) increasingly deviate from the results with  $\varphi = 0$  (not illustrated here). The same is true as  $\varphi$  decreases from 0 to  $-0.007$ , with the results  $\varphi = -0.007$  being similar to those shown for the other extremum ( $\varphi = 0.067$ ) in Figure 6.

*Experiment #4: Dilation of eigenvalues of  $A^{(s)}$ .* In this experiment, once again, the V-shaped model (see Figure 3 and Table 1) is adopted in the synthesis of the  $\ell_x = 3$ -dimensional state process,  $x_t$ , and of the two  $\ell_y = 2$ -dimensional bivariate data channels,  $d_{s,t}$  and  $d_t$ , for the system in (33), with  $r = 10^{-3}$ ,  $\rho = 10^{-5}$  (42),  $\underline{t} = 200$ ,  $\bar{t} = 400$ , MC = 500. This system has 3 distinct real eigenvalues, which suffer a common dilation (i.e. scaling) mismatch in the target's analysis model,  $A^{(a)}$ ; i.e. the target adopts the state transition matrix,  $A^{(a)} = \sigma A^{(s)} = \sigma A$  (33), with  $\sigma = 1.4$  (Section 4.1.2). Figure 7 displays all four performance measures defined in Section 4.4. We note the following:

- (i) FPD-BTL exhibits strongly positive transfer below threshold (i.e. for  $r_s > 10r$  in this  $n_s = 1$  case), which is explained in the next paragraph.
- (ii) For a wide range of  $r_s/r$ , of FPD-BTL performs better than the other methods.
- (iii) Both methods based on complete modelling (i.e. BCM and DSMF) have a similar TNSE (Figure 7a).
- (iv) DSMF exhibits negative transfer below threshold (Figure 7b).

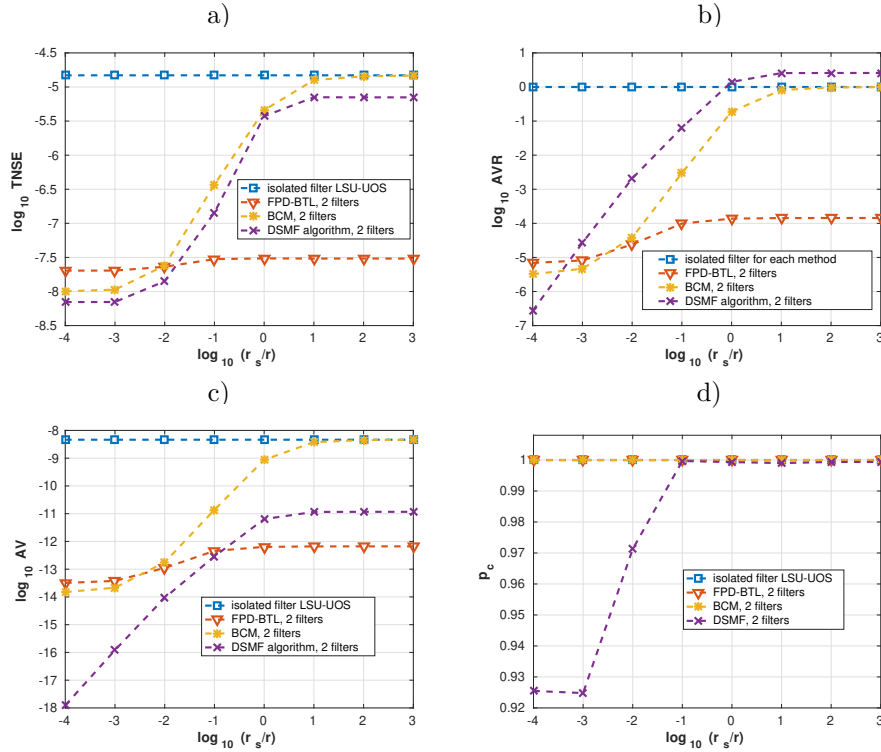


Figure 7: Experiment #4: a) TNSE (38), b) AVR (40), c) AV (39) and d)  $p_c$  (41), with dilation— $\sigma = 1.4$ —of the of eigenvalues of  $A$  (33) in the target analysis model (FPD-BTL), and in the complete analysis model (BCM and DSMF. V-shaped complete model (Figure 3a)).

- (v) The containment probability,  $p_c$ , for DSMF rapidly falls (i.e. deteriorates) above threshold at  $r_s = 0.1 r$  (Figure 7). The Bayesian methods maintain  $p_c = 1, \forall r_s/r$ .

There is an apparent saturation of the FPD-BTL performance below threshold (Figures 7a–c); i.e. those FPD-BTL performance measures are far better (lower) than those of the isolated filter, as  $r_s/r$  increases, but saturating below threshold. This can be explained in the following way: if the source observation noise,  $r_s$ , is high, its local data update (22) via  $y_{s,t}$  provides no learning/concentration for  $x_{s,t}$ , because the source data strip (21), (22) is a superset of the filtering inference (23) prior state predictor’s orthotope (24). Therefore, the source evolves only via time updates. Effectively, its uncertainty increases each step by the state noise half-width,  $\rho$  (42). For  $\rho$  large, the measure of the source posterior support (23) grows quickly, and the transferred state predictor brings no more knowledge to the target, after some filtering horizon,  $t_H < \bar{t}$ . In his case, the target effectively becomes isolated from the source for  $t > t_H$ . For  $\rho$  small, the filtering uncertainty (23) grows more slowly, and, effectively,  $t_H > \bar{t}$ . Had we increased  $\bar{t}$  to  $t_H$  sufficiently, the FPD-BTL performances would,

indeed, have saturated at those if the isolated target, confirming that FPD-BTL is, indeed, robust.

As  $\sigma$  increases from 1 (analysis-synthesis matching) to 1.4, the deviations of the performance measures from those at  $\sigma = 1$  increase (not illustrated). For  $\sigma < 1$  and  $\sigma > 1.4$ , these deviations are insensitive to  $\sigma$  as well, i.e. the effect of the eigenvalue dilation is most significant in the interval  $1 < \sigma < 1.4$ .

Finally, note that these findings are influenced only minimally by non-isotropic dilation of the eigenvalues of  $A^{(s)}$  (33), for instance the case in which only the largest-radius eigenvalue is perturbed by *sigma*.

*Experiment #5: State noise mismatch.* Here, the U-shaped synthesis model (Figure 3b) is adopted with system (33), modified so that  $A^{(s)} \equiv 1.4$ . The operating parameter,  $\alpha > 0$  (31), therefore controls the mismatch in the target’s analytic model for  $x_t$  in FPD-BTL (Figure 3c) (i.e. the target filter adopts  $e_t = 0$  in (31)), as well as in the complete modelling (BCM and DSMF) which assume a V-shaped analysis model (see Figure 3a and Section 4.1.1). Specifically, in this experiment,  $\alpha = 0.4$ , which was found to induce the maximal state mismatch for which the FPD-BTL algorithm remained numerically stable. Also,  $r = 10^{-3}$ ,  $\rho = 10^{-2}$ ,  $\underline{t} = 50$ ,  $\bar{t} = 400$ , MC = 200 runs. All four performance measures (Section 4.4) are graphed in Figures 8a–d respectively. We note the following:

- (i) The scale of the vertical axis in Figure 8a is far smaller than in the TNSE graphs at earlier experiments; i.e. positive transfer is far smaller than in those earlier experiments. Also, Figures 8b and 8c show similarly small positive transfer for the Bayesian methods (FPD-BTL and BCM).
- (ii) In Figure 8a, the complete modelling cases (BCM and DSMF) have opposing trends to those in earlier experiments. Furthermore, BCM exhibits negative transfer (for TNSE) *above* threshold.
- (iii) DSMF has negative transfer below threshold (Figure 8b).
- (iv) Although DSMF exhibits a significant reduction in estimate uncertainty above threshold (Figure 8c), its containment probability,  $p_c$ , falls to zero in this regime (Figure 8d). This underlines the fact that AVR and AV can be a misleading performance measures if quoted in the absence of  $p_c$ .

This experiment demonstrates that all the tested alternatives to our FPD-BTL algorithm perform unreliably when exposed to state noise mismatch in the analysis model. In contrast, FPD-BTL demonstrates robustness below the observation noise threshold,  $r_s > 10r$ , and weakly positive transfer above threshold.

#### 4.6. Computational costs of the filtering algorithms

To assess the relative computational costs of the 3 algorithms,  $n = 2$  scalar observation channels are synthesized via the V-shaped graph (Figure 3a) with system (32). Common state process,  $x_t$  (15), is sequentially estimated via FPD-BTL (Algorithm 1), and by the fully-modelled alternatives (BCM, Section 4.3.1, and DSMF, Section 4.3.2), now suppressing all the mismatches in

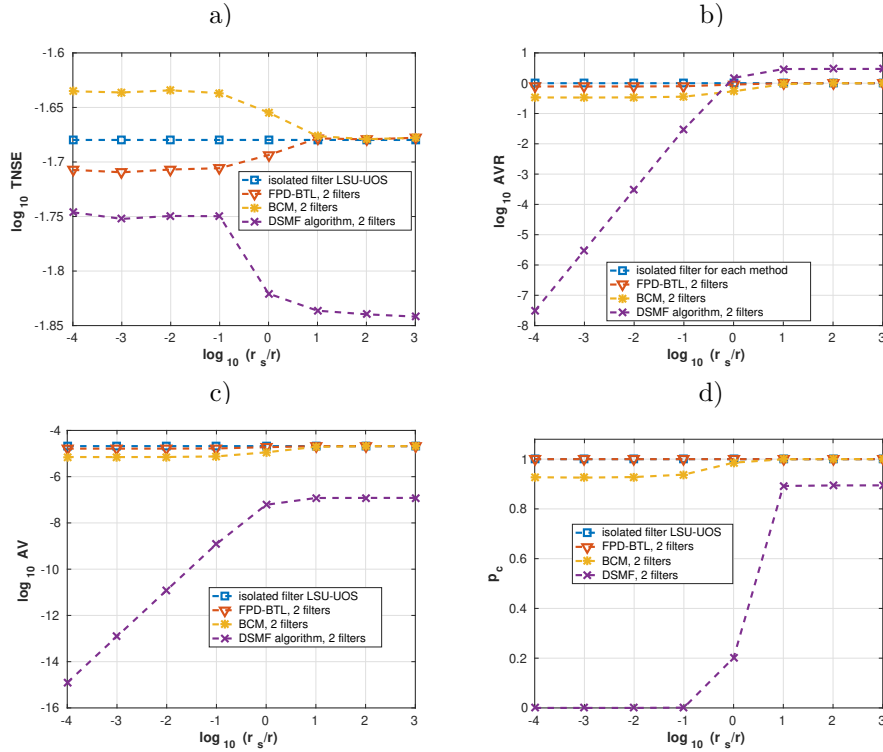


Figure 8: Experiment #5: a) TNSE (38), b) AVR (40), c) AV (39) and d)  $p_c$  (41) for a U-shaped synthesis model (Figure 3b) with  $\alpha = 0.4$  (31) and system (33) with  $A^{(s)} = A_S^{(a)} = A^{(a)} = 1.4A$ . State analysis model mismatches in FPD-BTL target filter ( $\alpha = 0$ ) and in the complete analysis models of BCM and DSMF (V-shaped graphs with  $\alpha = 0$ ).

analysis which we studied in Section 4.5. The algorithms are implemented in Matlab 2016a on an Intel i5-7500, 3.4 GHz machine hosting Linux operating system. All algorithms are run sequentially (no parallel processing).  $\bar{t} = 1000$  and  $MC = 1000$  runs per setting of  $r_s$  (there were 8 such settings). The runtimes were 946 s (FPD-BTL), 625 s (BCM) and 1605 s (DSMF). The comparative run-time for the isolated LSU-UOS filtering algorithm (23), (24) processing only scalar target data channel,  $d_t$  (Figure 3c), was 598 s.

With  $n \geq 2$  observation channels, BCM and DSMF compute just one time update per  $n$  data updates per step of these algorithms. A fusion operation is also required in every step of DSMF. Meanwhile, in FPD-BTL, the source and target tasks each involve one data- and time-update step (lines II. and III. in Algorithm 1, respectively), with the single transfer being computationally trivial (set intersection (26)). Note also that FPD-BTL requires only that a UOS state predictor,  $f_s(x_{s,t}|d_s(t-1))$  (24) be made available to the target in each step in the algorithm (line I. of Algorithm 1), but does not stipulate how the source actually calculates this. In this sense, the source data- and time-updates

can be omitted from the target’s computational budget, approximately halving the FPD-BTL runtime quoted above, and significantly outperforming the completely modelled alternatives (BCM and DSMF), which are centralized algorithms. This parallel nature of the FPD-BTL algorithm—parallelizable filtering operations with a trivial fusion/transfer operation (i.e. intersection) at the central target task—is a key attribute, recommending FPD-BTL in resource-critical applications that arise in sensorized environments [30].

#### 4.7. Discussion

The key distinction between our optimal Bayesian transfer learning algorithm (FPD-BTL), and the fully-modelled Bayesian (BCM) and fusion (DSMF) alternatives, lies in the fact that the source LSU-UOS task is an independent modeller, transferring only its local state predictor,  $f_s(x_{s,t}|d_s(t-1))$  (6)—i.e. its local (approximate) Bayesian sufficient statistics,  $\underline{x}_t^+$  and  $\bar{x}_t^+$  (24)—for processing by the target task. Our aim with these experiments has been to assess whether this provides robustness to mismatches that can affect the fully modelled alternatives, since FPD-BTL allows expert local (and independent) source knowledge to be transferred in support of the target.

We empirically defined a *threshold* using the source observation noise parameter,  $r_s$ , and the target observation noise parameter,  $r$  (42), at  $r_s = 10r$  for  $n_s = 1$  source (see, for example, Figure 5). FPD-BTL has *positive transfer* above threshold ( $r_s \leq 10r$ ) and it is *robust* (i.e. the transfer is rejected and the target reverts to an isolated LSU-UOS task) below threshold ( $r_s \geq 10r$ ). In the multi-source case ( $n_s > 1$ ), the threshold depends on  $n_s$  as  $r_s = 10n_s r$  (see Figure 4).

In the case of two filtering tasks ( $n = n_s + 1 = 2$ ), with matching of the synthetic and analytic models in both filters, FPD-BTL is robust below threshold and shows positive transfer above threshold, where its performance measures—TNSE (38), AVR (39) and AV (40)—saturate (Figure 5). The complete modelling methods (BCM and DSMF) saturate only in TNSE and not in uncertainty measures (AVR and AV), where they depend on  $r_s$  linearly, since they process raw source observations,  $y_{s,t}$ , using the source’s known observation model (both of which do not need to be processed in FPD-BTL). Also, if the synthetic and analytic models match, the DSMF algorithm yields improved TNSE below threshold, compared to BCM, due to tighter geometric approximation of the state set,  $\mathbb{X}_t$  (Section 4.4), by a general ellipsoid than by a (conservative) orthotope.

The DSMF algorithm needs a burn-in period because it is more sensitive to its initialization, unlike the Bayesian LSU-UOS methods. Therefore, the lower bound for the performance evaluation epoch had to be set as  $\underline{t} \gg 1$  for DSMF in section 4.4. Practically,  $\underline{t} = \bar{t}/2$  was used. Without this burn-in, the performance criteria for DSMF were all much worse, and, in fact, suffered a negative transfer.

In Section 4.5.3, we studied synthesis-analysis matching in the source ( $n_s = 1$ ) and mismatching in the target. FPD-BTL maintained its positive transfer above threshold and robustness below threshold in all the studied cases,

including sure containment probability,  $p_c = 1$  (41). Deterioration of filtering performance for the complete modelling methods (BCM and DSMF)—and their non-robustness to modelling mismatch—occurred in different ways, depending on the particular system and type of mismatch. For instance, note the greatly increased positive transfer in FPD-BTL vs BCM in Figure 6; in FPD-BTL vs both BCM and DSMF in Figures 7 and 8; note the negative transfer in Figures 7b (DSMF), 8a (BCM), and 8b (DSMF), compared to positive and robust transfer performance in FPD-BTL in these experiments; and, finally, note this  $p_c \rightarrow 0$  for DSMF in Figure 8d, while it remains at unity for FPD-BTL.

The state support set intersections, (22) and (26), were never empty if the target synthesis and analysis models matched. However, in the cases of target model mismatch (Section 4.5.3), the values of the mismatch operating parameters ( $\varphi$  in Experiment #3,  $\sigma$  in Experiment #4, and  $\alpha$  in Experiment #5) were chosen appropriately, so that the target synthesis and analysis models did not differ excessively. Otherwise, the intersections, (22) and (26), may have been empty, and transfer stopped (Theorem 1, final statement). It was observed that intersections in the data update (22) had a tendency to be empty more often (and it was more sensitive to inappropriate values of the operating parameters) than in the transfer (26). In experiments, these cases checked and discarded.

In summary, the FPD-BTL algorithm has the following properties:

- it does not require a complete model of the source, nor its interaction with the target;
- in analysis, the source and target are independent tasks (multiple modelling),
- it requires transfer only of the UOS source state predictor (24) as a local expert Bayesian sufficient statistic for processing by the target; these statistics— $\underline{x}_t^+$  and  $\underline{x}_t^-$ —summarize all that is relevant in  $d_s(t)$ ,  $A_s$ ,  $B_s$ ,  $C_s$ , for transfer learning in the target;
- in the case of target analysis model mismatch, the target accepts the source state predictor, avoiding imposition of this mismatch on the source, as occurs in the complete modelling strategies (BCM and DSMF);
- it readily scales to transfer of state predictors from multiple ( $n_s > 1$ ) sources;
- its threshold occurs at  $r_s = 10 n_s r$ , where  $n_s$  is number of sources; therefore, increasing the number of sources can compensate for poorer quality of individual source filters;
- the containment probability,  $p_c$ , is unity and never collapses, even when the target analysis and synthesis models mismatch;
- the computational costs of FPD-BTL at the target are far smaller than the costs of the complete modelling methods at the processing/fusion centre.

Local data are processed locally (intrinsic parallelization), and the FPD-optimal BTL operator for LSU-UOS class—i.e. the required minimization of Kullback-Leibler divergence—reduces to intersection of supporting orthotopes at the target.

## 5. Conclusion

In this paper, we have proposed a Bayesian transfer learning (BTL) algorithm based on fully probabilistic design (FPD), and have applied it to transfer between filtering tasks described by linear state-space models with uniformly distributed noises on orthotopic support (i.e. LSU-UOS filters).

As already noted, FPD-BTL is truly a *transfer* learning technique, as opposed to a joint/multi-channel inference scheme, since the source is an independent modeller from the target (multiple modelling) and it transfers the result of its local Bayesian inference task—state prediction—to support the inference task (i.e. state filtering) at the target, in line with the core notions of transfer learning [6]. FPD-BTL is also a truly *Bayesian* transfer learning algorithm, where the source’s fully probabilistic inference,  $f_s(x_{s,t}|d_s(t-1))$  (Figure 1), is transferred, rather than the source data,  $d_s(t)$ , or merely their statistics. Therefore, a hallmark of BTL is that the target processes the source’s (Bayesian) sufficient statistics and local modelling knowledge,  $f_s(\cdot)$ , rather than requiring the transfer of the raw source data. We can see this, for instance, in the second line of transfer step I. in Algorithm 1, which processes UOS state predictor (24), with shaping parameters (statistics),  $\underline{x}_{t+1}^+$  and  $\bar{x}_{t+1}^+$ , rather than the joint processing of  $d_s(t)$  and  $d(t)$  in BCM (35).

FPD-BTL generally involves mean-field-type integrals which can be hard to compute. Its specialisation in LSU-UOS filtering tasks results in the FPD-justified geometric intersection operator for the transfer step, which is computationally trivial for orthotopes. Moreover, this operator can be readily extended to multiple source tasks (Theorem 4), with exceptional implementational speed (i.e. minimal increase in computational cost with  $n_s > 1$  ).

The proposed BTL operator is a function of the source uncertainty (measured as variance or entropy), and not simply the source’s state estimate. It is this which enables robust transfer, i.e. the rejection of poor-quality source knowledge. In addition, the application of FPD-BTL to the UOS class has proved to be theoretically significant, since it demonstrates that the non-robustness of earlier Gaussian-based FPD-optimal BTL schemes, e.g. in [39], is a consequence of higher-moment loss in the induced mean-field operator, and is not an intrinsic limitation of FPD methodology.

Finally, note that the the proposed BTL technique can be used to transfer from any source learning tasks (filters) that yield sequential state predictors, including particle filters, point-mass filters, etc.

The results presented here can be further developed in the following ways:

- Currently, there is no measure of trust in the reliability of the source(s): the target fully accepts the source knowledge (6). The future research will

focus on the target’s (Bayesian) modelling of the sources’ reliability.

- Further research is required into the case where the sets in the transfer (26) and data updates (22) are disjoint. This can probably be resolved via a sub-unity transfer weight.
- The isolated LSU-UOS filtering algorithm (Section 3.1) comprises two local approximations per filtering step. The accumulated approximation error can be reduced via more flexible geometric support approximations, such as zonotopes [48], [49], with bounding guarantees available via global approximations based on empirical approximations (e.g. particle filters [31]).
- In future work, the target can itself be a joint network modeller, independent of the source(s), as in [18], further enhancing the positive transfer.
- The currently adopted FPD-BTL scheme involves static transfer, in the sense that the source knowledge is transferred in the form of the marginal state predictor at each time step. By transferring joint distributions over multiple time steps—i.e. dynamic transfer—the source’s temporal (dynamic) knowledge can be exploited at the target [43].

## Acknowledgment

This research has been supported by The Czech Science Foundation (GAČR) [grant 18-15970S].

## Appendix A. Proofs

### Appendix A.1. Proof of Theorem 1

Let us partition the integration domain,  $\mathbb{X}_{s,t}$ , of  $f_s(x_t|d_s(t-1))$  into sets  $\mathbb{X}_t^\cap$  and  $\mathbb{X}_t^\bullet$  (see Figure 2), so that  $\mathbb{X}_t^\cap = \mathbb{X}_{s,t} \cap \mathbb{X}_t$  and  $\mathbb{X}_t^\bullet = \mathbb{X}_{s,t} \cap \mathbb{X}_t^c$ , where  $\mathbb{X}_t^c$  is the complement of  $\mathbb{X}_t$ . Alternatively:  $\mathbb{X}_t^\cap = \{x_t | x_t \in \mathbb{X}_{s,t} \wedge x_t \in \mathbb{X}_t\}$  and  $\mathbb{X}_t^\bullet = \{x_t | x_t \in \mathbb{X}_{s,t} \wedge x_t \notin \mathbb{X}_t\}$ . It holds that  $\mathbb{X}_t^\cap \cap \mathbb{X}_t^\bullet = \emptyset$  and  $\mathbb{X}_t^\cap \cup \mathbb{X}_t^\bullet = \mathbb{X}_{s,t}$ . The set,  $\mathbb{X}_t^\bullet$ , is open on the border with  $\mathbb{X}_t$ , i.e.  $\mathbb{X}_t^\bullet \cap \mathbb{X}_t = \emptyset$ .

Also,  $\mathbb{Y}_t|x_t$  is the support of  $f(y_t|x_t)$  and  $\check{\mathbb{Y}}_t|x_t$  of  $\check{f}(y_t|x_t, f_s)$ , both a function of  $x_t$ . The set  $\mathbb{Y}_t|x_t \neq \emptyset, \forall x_t \in \mathbb{R}^{\ell_x}$ , (19).

The KLD (12) can be written, using Fubini’s theorem, as

$$D(\check{f} \parallel f^I) = \int_{\mathbb{X}_{s,t}} f_s(x_t|d_s(t-1)) D_y(x_t) dx_t + D_{x_1} + D_{x_2}, \quad (\text{A.1})$$

where

$$\begin{aligned} D_y(x_t) &= \int_{\check{\mathbb{Y}}_t|x_t} \check{f}(y_t|x_t, f_s) \ln \frac{\check{f}(y_t|x_t, f_s)}{f(y_t|x_t)} dy_t, \\ D_{x1} &= \int_{\mathbb{X}_t^\cap} f_s(x_t|d_s(t-1)) \ln \frac{f_s(x_t|d_s(t-1))}{f(x_t|d(t-1))} dx_t, \\ D_{x2} &= \int_{\mathbb{X}_t^\bullet} f_s(x_t|d_s(t-1)) \ln \frac{f_s(x_t|d_s(t-1))}{f(x_t|d(t-1))} dx_t. \end{aligned}$$

Let us consider three (exhaustive) cases of the relationship between the sets  $\mathbb{X}_{s,t}$  and  $\mathbb{X}_t$ :

- (i)  $\mathbb{X}_{s,t} \subseteq \mathbb{X}_t$ , i.e.  $\mathbb{X}_t^\bullet = \emptyset$ , which is a special case (Figure 2, case (i)). Then  $D_{x2} = 0$ . Also,  $D_{x1}$  is a non-negative, finite constant independent of  $\check{f}(y_t|x_t, f_s)$ . The only term influencing  $D(\check{f} \| f^I)$  is  $D_y(x_t)$ . To be finite, it must hold that  $\check{\mathbb{Y}}_t|x_t \subseteq \mathbb{Y}_t|x_t$ , where  $\mathbb{Y}_t|x_t$  is the support of  $f(y_t|x_t)$ . To minimize  $D_y(x_t)$ , we must minimize the normalization constant of  $\check{f}(y_t|x_t)$ , i.e. extend maximally the support of  $\check{f}(y_t|x_t, f_s)$  to maximize its measure relating  $\check{\mathbb{Y}}_t|x_t = \mathbb{Y}_t|x_t$ . Then,  $f^o(y_t|x_t, f_s) \propto f(y_t|x_t)$ , given  $x_t \in \mathbb{X}_t^\cap$  ( $\equiv \mathbb{X}_{s,t}$ ). After substitution into (11), the FPD-optimal joint pdf  $f^o \propto f(y_t|x_t) f_s(x_t|d_s(t-1))$ , i.e. it is zero  $\forall x_t \notin \mathbb{X}_t^\cap$ .
- (ii)  $(\mathbb{X}_{s,t} \not\subseteq \mathbb{X}_t) \wedge (\mathbb{X}_{s,t} \cap \mathbb{X}_t \neq \emptyset)$ , i.e. both  $\mathbb{X}_t^\cap$  and  $\mathbb{X}_t^\bullet$  are non-empty (Figure 2, case (ii)). In this general case, we adopt  $f^o(y_t|x_t, f_s) \propto f(y_t|x_t)$ ,  $\forall x_t \in \mathbb{X}_t^\cap$ , in consequence of (i), and prove its optimality here. We introduce the following sequences,  $k \in \mathbb{N}$ :

- $f^{(k)}(x_t|d(t-1)) > 0$ ,  $\forall x_t \in \mathbb{R}^{\ell_x}$  and  $\forall k$ , with  $\lim_{k \rightarrow +\infty} f^{(k)}(x_t|d(t-1)) = f(x_t|d(t-1))$ ,
- $\check{f}^{(k)}(y_t|x_t, f_s) \propto f(y_t|x_t) \xi^{(k)}(x_t)$ , where  $\xi^{(k)}(x_t) > 0$ ,  $\forall x_t \in \mathbb{R}^{\ell_x}$  and  $\forall k$ , with  $\lim_{k \rightarrow +\infty} \xi^{(k)}(x_t) = \chi(x_t \in \mathbb{X}_t^\cap)$ .

These sequences converge to uniform pdfs.

The sequences defined above are chosen so that  $0 < \frac{\check{f}^{(k)}(y_t|x_t, f_s)}{f^{(k)}(x_t|d(t-1))} \leq a^{(k)} < +\infty \forall x_t \in \mathbb{X}_{s,t}$ ,  $y_t \in \check{\mathbb{Y}}_t|x_t$  and  $\lim_{k \rightarrow +\infty} a^{(k)} < +\infty$ . This choice guarantees a finite KLD (12).

The definitions above imply

$$\begin{aligned} D_y^{(k)}(x_t) &= \int_{\check{\mathbb{Y}}_t|x_t} \check{f}^{(k)}(y_t|x_t, f_s) \ln \frac{\check{f}^{(k)}(y_t|x_t, f_s)}{f(y_t|x_t)} dy_t, \\ D_{x_1}^{(k)} &= \int_{\mathbb{X}_t^\square} f_s(x_t|d_s(t-1)) \ln \frac{f_s(x_t|d_s(t-1))}{f^{(k)}(x_t|d(t-1))} dx_t. \end{aligned}$$

We define the sequence,  $D(\check{f} \| f^I)^{(k)}$ , where  $\lim_{k \rightarrow +\infty} D(\check{f} \| f^I)^{(k)} = D(\check{f} \| f^I)$ , and, similarly to (A.1), we can express it formally as

$$\begin{aligned} D(\check{f} \| f^I)^{(k)} &= \underbrace{\int_{\mathbb{X}_t^\square} f_s(x_t|d_s(t-1)) D_y^{(k)}(x_t) dx_t + D_{x_1}^{(k)}}_{S^{(k)}} + \\ &+ \underbrace{\int_{\mathbb{X}_t^\bullet} f_s(x_t|d_s(t-1)) \int_{\check{\mathbb{Y}}_t|x_t} \check{f}^{(k)}(y_t|x_t, f_s) \ln \frac{f_s(x_t|d_s(t-1))}{f(y_t|x_t)} dy_t dx_t}_{Q^{(k)}} + \\ &+ \underbrace{\int_{\mathbb{X}_t^\bullet} f_s(x_t|d_s(t-1)) \int_{\check{\mathbb{Y}}_t|x_t} \check{f}^{(k)}(y_t|x_t, f_s) \ln \frac{\check{f}^{(k)}(y_t|x_t, f_s)}{f^{(k)}(x_t|d(t-1))} dy_t dx_t}_{R^{(k)}}. \end{aligned} \tag{A.2}$$

The term  $S^{(k)}$  in (A.2) can be taken directly to the limit ( $k \rightarrow +\infty$ ) and treated as in case (i), with the optimal result  $f^o \propto f(y_t|x_t) f_s(x_t|d_s(t-1))$ ,  $\forall x_t \in \mathbb{X}_t^\square$ . According to the definitions of the sequences,  $\check{f}^{(k)}(y_t|x_t, f_s)$  and  $f^{(k)}(x_t|d(t-1))$ , and recalling that  $\mathbb{X}_t^\bullet$  is open, the terms  $Q^{(k)}$  and  $R^{(k)}$  in (A.2) converge pointwise to zero for  $x_t \in \mathbb{X}_t^\bullet$ . Therefore, if  $k \rightarrow +\infty$ , KLD (A.2) is finite  $\forall x_t \in \mathbb{X}_t^\bullet$ . Hence, given  $x_t \in \mathbb{X}_t^\bullet$ ,  $f^o(y_t|x_t, f_s) = \lim_{k \rightarrow +\infty} \check{f}^{(k)}(y_t|x_t, f_s) = 0$  for all  $y_t \in \mathbb{R}^{\ell_y}$ , i.e.  $\check{f} = 0$  for  $x_t \in \mathbb{X}_t^\bullet$ . If  $x_t \notin \mathbb{X}_{s,t}$ , then  $\check{f} = 0$  also (11). Without changing  $\check{f}$ , we can define  $f^o(y_t|x_t, f_s) \propto f(y_t|x_t) \chi(x_t \in \mathbb{X}_t^\square)$ .

- (iii)  $\mathbb{X}_{s,t} \cap \mathbb{X}_t = \emptyset$ , then  $\mathbb{X}_t^\square = \emptyset$  and  $f^o(y_t|x_t, f_s) \equiv 0$ ,  $\forall x_t \in \mathbb{R}^{\ell_x}$  (Figure 2, case (iii)). In this case, as a consequence of the target's full trust in the source's state predictor (see the first bullet point in Section 5), transfer learning is impossible and we define  $f^o(y_t|x_t, f_s) \equiv f(y_t|x_t)$ , i.e.  $f^o(y_t|x_t, f_s)$  is conditionally independent of  $f_s$ , and  $\mathbb{X}_t^o \equiv \mathbb{X}_t$ .

To conclude the proof, if  $\mathbb{X}_t^\square = \emptyset$ , then the sought pdf,  $f^o(y_t|x_t, f_s)$ , conditioned on the transferred source state predictor,  $f_s$ , is proportional to  $f(y_t|x_t)$ ,

if  $x_t \in \mathbb{X}_t^\cap$ , and it is zero if  $x_t \notin \mathbb{X}_t^\cap$ ; i.e.  $f^o(y_t|x_t, f_s) \propto f(y_t|x_t \in (\mathbb{X}_{s,t} \cap \mathbb{X}_t))$ . Hence,  $\mathbb{X}_t^o = \mathbb{X}_t^\cap$ . Conversely, if  $\mathbb{X}_t^\cap = \emptyset$ , then  $f^o(y_t|x_t, f_s) \equiv f(y_t|x_t)$  (i.e. the isolated target observation model) and  $\mathbb{X}_t^o \equiv \mathbb{X}_t$ .

#### Appendix A.2. Proof of Theorem 4

Let  $n = 3$ . The filter 1 is the target filter and filters 2 and 3 are the source filters. Perform transfer learning between the filters 2 and 3 by intersecting their state supports (Theorem 1). We obtain an abstract filter providing all the knowledge in filters 2 and 3 available for transfer to filter 1. The transfer between the abstract filter and filter 1, then results in another intersection. As intersection is a commutative and associative operation, we obtain (30). The same procedure can be applied for any  $n \geq 3$ .

## References

- [1] H. Fourati, *Multisensor data fusion: from algorithms and architectural design to applications*. CRC press, 2017.
- [2] A. Diez-Olivan, J. Del Ser, D. Galar, and B. Sierra, “Data fusion and machine learning for industrial prognosis: trends and perspectives towards industry 4.0,” *Information Fusion*, vol. 50, pp. 92 – 111, 2019.
- [3] M. B. Alatise and G. P. Hancke, “A Review on Challenges of Autonomous Mobile Robot and Sensor Fusion Methods,” *IEEE ACCESS*, vol. 8, pp. 39830–39846, 2020.
- [4] F. Castanedo, “A Review of Data Fusion Techniques,” *Scientific World Journal*, 2013.
- [5] Y. Zheng, “Methodologies for cross-domain data fusion: an overview,” *IEEE Transactions on Big Data*, vol. 1, pp. 16–34, 2015.
- [6] S. J. Pan and Q. Yang, “A survey on transfer learning,” *IEEE Transactions on Knowledge and Data Engineering*, vol. 22, no. 10, pp. 1345–1359, 2010.
- [7] R. Ouyang and B. K. H. Low, “Gaussian process decentralized data fusion meets transfer learning in large-scale distributed cooperative perception,” *Autonomous Robots*, vol. 44, no. 3, pp. 359–376, 2020.
- [8] Q. Wang and J. Zhang, “A data transfer fusion method for discriminating similar spectral classes,” *Sensors*, vol. 16, no. 11, 2016.
- [9] N. Hernandez-Cruz, M. Razzaq, C. Nugent, I. McChesney, and S. Zhang, “Transfer learning and data fusion approach to recognize activities of daily life,” in *Proceedings of the 12th EAI International Conference on Pervasive Computing Technologies for Healthcare*, pp. 227–231, 2018.

- [10] H. Lin, J. Hu, W. Xiaoding, M. F. Alhamid, and M. Jalil Piran, “Towards secure data fusion in industrial IoT using transfer learning,” *IEEE Transactions on Industrial Informatics*, 2020.
- [11] S. Beddar-Wiesing and M. Bieshaar, “Multi-sensor data and knowledge fusion—a proposal for a terminology definition,” *arXiv preprint arXiv:2001.04171*, 2020.
- [12] J. Lu, V. Behbood, P. Hao, H. Zuo, S. Xue, and G. Zhang, “Transfer learning using computational intelligence: A survey,” *Knowledge-Based Systems*, vol. 80, pp. 14–23, 2015.
- [13] A. Karbalayghareh, X. Qian, and E. R. Dougherty, “Optimal Bayesian transfer learning,” *IEEE Transactions on signal processing*, vol. 66, no. 14, pp. 3724–3739, 2018.
- [14] R. Chandra and A. Kapoor, “Bayesian neural multi-source transfer learning,” *Neurocomputing*, vol. 378, pp. 54 – 64, 2020.
- [15] K. Wang and F. Tsung, “Bayesian cross-product quality control via transfer learning,” *International Journal of Production Research*, pp. 1–19, 2020.
- [16] H. Li, F. Wang, H. Li, and Q. Wang, “Safety control modeling method based on Bayesian network transfer learning for the thickening process of gold hydrometallurgy,” *Knowledge-Based Systems*, vol. 192, 2020.
- [17] A. Wilson, A. Fern, and P. Tadepalli, “Transfer learning in sequential decision problems: a hierarchical Bayesian approach,” in *Proceedings of ICML Workshop on Unsupervised and Transfer Learning*, pp. 217–227, 2012.
- [18] M. Papež and A. Quinn, “Transferring model structure in Bayesian transfer learning for Gaussian process regression,” *arXiv preprint arXiv:2101.06884*, 2021.
- [19] S. Kullback and R. Leibler, “On information and sufficiency,” *Annals of Mathematical Statistics*, vol. 22, pp. 79–87, 1951.
- [20] A. Quinn, M. Kárný, and T. Guy, “Fully probabilistic design of hierarchical Bayesian models,” *Information Sciences*, vol. 369, no. 1, pp. 532–547, 2016.
- [21] A. d’Onofrio, *Bounded Noises in Physics, Biology, and Engineering*. Springer, 2013.
- [22] L. Jirsa, L. Kuklišová Pavelková, and A. Quinn, “Knowledge transfer in a pair of uniformly modelled Bayesian filters,” in *Proceedings of the 16th International Conference on Informatics in Control, Automation and Robotics - Volume 1*, pp. 499–506, INSTICC, SciTePress, 2019.

- [23] L. Jirsa, L. Kuklišová Pavelková, and A. Quinn, “Bayesian transfer learning between uniformly modelled Bayesian filters,” in *Informatics in Control, Automation and Robotics* (O. Gusikhin, K. Madani, and J. Zaytoon, eds.), vol. 720 of *Lecture Notes in Electrical Engineering*, (Cham), pp. 151–168, Springer International Publishing, 2021.
- [24] Z. Wang, X. Shen, and Y. Zhu, “Ellipsoidal Fusion Estimation for Multisensor Dynamic Systems With Bounded Noises,” *IEEE Transactions on Automatic Control*, vol. 64, no. 11, pp. 4725–4732, 2019.
- [25] Q. Shen, J. Liu, X. Zhou, W. Qin, L. Wang, and Q. Wang, “Centralized Fusion Methods for Multi-Sensor System With Bounded Disturbances,” *IEEE ACCESS*, vol. 7, pp. 141612–141626, 2019.
- [26] Y. Becis-Aubry, “Multisensor fusion for state estimation of linear models in the presence of bounded disturbances,” in *Proceedings of the American Control Conference*, pp. 6781–6782, IEEE, 2010.
- [27] C. Yuan and F. Wu, “Cooperative state estimation of multi-agent systems subject to bounded external disturbances,” *International Journal of Systems Science*, vol. 49, no. 9, pp. 1985–1996, 2018.
- [28] N. Xia, F. Yang, and Q.-L. Han, “Distributed networked set-membership filtering with ellipsoidal state estimations,” *Information Sciences*, vol. 432, pp. 52–62, 2018.
- [29] U. D. Hanebeck and J. Horn, “Fusing information simultaneously corrupted by uncertainties with known bounds and random noise with known distribution,” *Information Fusion*, vol. 1, pp. 55–63, 2000.
- [30] B. Chen, D. W. C. Ho, W. Zhang, and L. Yu, “Networked fusion estimation with bounded noises,” *IEEE Transactions on Automatic Control*, vol. 62, no. 10, pp. 5415–5421, 2017.
- [31] W. Li, Z. Wang, Y. Yuan, and L. Guo, “Particle filtering with applications in networked systems: a survey,” *Complex and Intelligent Systems*, vol. 2, pp. 293–315, 2016.
- [32] G. M. Hoang, B. Denis, J. Härrri, and D. T. M. Slock, “Select thy neighbors: Low complexity link selection for high precision cooperative vehicular localization,” in *2015 IEEE Vehicular Networking Conference (VNC)*, pp. 36–43, 2015.
- [33] Z. Wang, X. Shen, Y. Zhu, and J. Pan, “Monte Carlo set-membership filtering for nonlinear dynamic systems,” in *2016 19th International Conference on Information Fusion*, pp. 1071–1078, 2016.
- [34] A. Balestrino, A. Caiti, and E. Crisostomi, “Particle filtering within a set-membership approach to state estimation,” in *14th Mediterranean Conference on Control and Automation*, p. 44–49, 2006.

- [35] M. Kárný, J. Böhm, T. V. Guy, L. Jirsa, I. Nagy, P. Nedoma, and L. Tesař, *Optimized Bayesian Dynamic Advising: Theory and Algorithms*. London: Springer, 2005.
- [36] M. Kárný and T. Kroupa, “Axiomatisation of fully probabilistic design,” *Information Sciences*, vol. 186, no. 1, pp. 105–113, 2012.
- [37] J. M. Bernardo, “Expected information as expected utility,” *The Annals of Statistics*, vol. 7, no. 3, pp. 686–690, 1979.
- [38] A. Quinn, M. Kárný, and T. Guy, “Optimal design of priors constrained by external predictors,” *International Journal of Approximate Reasoning*, vol. 84, no. 1, pp. 150–158, 2017.
- [39] C. Foley and A. Quinn, “Fully probabilistic design for knowledge transfer in a pair of Kalman filters,” *IEEE Signal Processing Letters*, vol. 25, pp. 487–490, 2018.
- [40] T. Söderström, *Discrete-time stochastic systems: estimation and control*. Springer Science & Business Media, 2002.
- [41] L. Jirsa, L. Kuklišová Pavelková, and A. Quinn, “Approximate Bayesian prediction using state space model with uniform noise,” in *Informatics in Control Automation and Robotics* (O. Gusikhin and K. Madani, eds.), vol. 613 of *Lecture Notes in Electrical Engineering*, pp. 552–568, Cham: Springer International Publishing, 2020.
- [42] L. Pavelková and L. Jirsa, “Approximate recursive Bayesian estimation of state space model with uniform noise,” in *Proceedings of the 15th International Conference on Informatics in Control, Automation and Robotics*, pp. 388–394, 2018.
- [43] M. Papež and A. Quinn, “Dynamic Bayesian knowledge transfer between a pair of Kalman filters,” in *2018 28th International Workshop on Machine Learning for Signal Processing (MLSP)*, (Aalborg, Denmark), pp. 1–6, IEEE, 2018.
- [44] A. W. v. d. Vaart, *Asymptotic Statistics*. Cambridge Series in Statistical and Probabilistic Mathematics, Cambridge University Press, 1998.
- [45] E. T. Jaynes, *Probability Theory: The Logic of Science*. Cambridge University Press, 2003.
- [46] D. Koller and N. Friedman, *Probabilistic graphical models: principles and techniques*. MIT press, 2009.
- [47] B. Friedland, *Control system design: An introduction to state-space methods*. Courier Corporation, 2012.

- [48] W. Tang, Z. Wang, Q. Zhang, and Y. Shen, “Set-membership estimation for linear time-varying descriptor systems,” *Automatica*, vol. 115, 2020. Open access.
- [49] J. K. Scott, D. M. Raimondo, G. R. Marseglia, and R. D. Braatz, “Constrained zonotopes: A new tool for set-based estimation and fault detection,” *Automatica*, vol. 69, pp. 126–136, 2016.